The Plant Cell, Vol. 26: 1308–1329, March 2014, www.plantcell.org

Golgi-Dependent Transport of Vacuolar Sorting Receptors Is Regulated by COPII, AP1, and AP4 Protein Complexes in Tobacco[W][OPEN]

David C. Gershlick, Carine de Marcos Lousa, Ombretta Foresti,[1] Andrew J. Lee, Estela A. Pereira,[2] Luis L.P. daSilva,[2] Francesca Bottanelli,[3] and Jurgen Denecke[4]

Centre for Plant Sciences, School of Biology, Faculty of Biological Sciences, University of Leeds, Leeds LS2 9JT, United Kingdom

The cycling of vacuolar sorting receptors (VSRs) between early and late secretory pathway compartments is regulated by signals in the cytosolic tail, but the exact pathway is controversial. Here, we show that receptor targeting in tobacco (*Nicotiana tabacum*) initially involves a canonical coat protein complex II–dependent endoplasmic reticulum-to-Golgi bulk flow route and that VSR–ligand interactions in the *cis*-Golgi play an important role in vacuolar sorting. We also show that a conserved Glu is required but not sufficient for rate-limiting YXXϕ-mediated receptor trafficking. Protein–protein interaction studies show that the VSR tail interacts with the μ-subunits of plant or mammalian clathrin adaptor complex AP1 and plant AP4 but not that of plant and mammalian AP2. Mutants causing a detour of full-length receptors via the cell surface invariantly cause the secretion of VSR ligands. Therefore, we propose that cycling via the plasma membrane is unlikely to play a role in biosynthetic vacuolar sorting under normal physiological conditions and that the conserved Ile-Met motif is mainly used to recover mistargeted receptors. This occurs via a fundamentally different pathway from the prevacuolar compartment that does not mediate recycling. The role of clathrin and clathrin-independent pathways in vacuolar targeting is discussed.

INTRODUCTION

Soluble vacuolar proteins of plants represent the major class of edible protein on Earth and, as such, one of the cornerstones of food security. While this class is mainly found in plant storage tissues such as seeds (Herman and Larkins, 1999; Vitale and Hinz, 2005), vacuolar proteins of vegetative tissues are often proteolytic enzymes or specific hydrolases involved in defense against microbial pathogens (Stintzi et al., 1993). Similar to secreted proteins, they are initially synthesized on the rough endoplasmic reticulum (ER) but are thought to selectively segregate from secreted proteins (Dorel et al., 1989). The deviation from the default pathway to the plasma membrane (PM; Denecke et al., 1990) has been suggested to occur via a variety of active signal-mediated pathways and associated branch points in the pathway (De Marcos Lousa et al., 2012).

One early branch point is thought to be at the level of the ER itself. Anterograde trafficking at this point is mediated by the so-called coat protein complex II (COPII), which highlights ER export sites (Barlowe et al., 1994; daSilva et al., 2004). The COPII machinery consists of the Sec23/24/13/31 tetramer, the GTPase Sar1, and its GEF Sec12. It has been suggested that other pathways may bypass the Golgi apparatus in so-called KDEL protein–containing vesicles for mass transport (Toyooka et al., 2000) or precursor-accumulating vesicles (Hara-Nishimura et al., 1998). Other than ultrastructural images of morphologically distinct membrane compartments carrying vacuolar cargo, no direct evidence has been presented to show how these carriers bud from the ER and which proteins (membrane spanning and/or cytosolic) help shape these structures. It is also unclear how large ER-derived structures could selectively incorporate vacuolar but not secreted proteins.

The *trans*-cisternae of the Golgi apparatus (*trans*-Golgi) and the physically separated partially coated reticulum (Tanchak et al., 1988) or *trans*-Golgi network (TGN) (Dettmer et al., 2006) are considered to be the main branch points for vacuolar cargo. Specific vacuolar sorting receptors (VSRs) recruit vacuolar but not secreted proteins into clathrin-coated vesicles (CCVs) destined for fusion with the prevacuolar compartment (PVC). VSRs, originally identified from isolated CCVs (Kirsch et al., 1994), are type I membrane proteins with a large lumenal ligand binding domain that interacts with vacuolar sorting signals in a pH- and calcium-dependent manner (Kirsch et al., 1994; Shimada et al., 2002).

Unlike the cargo, which contains signals for vacuolar transport only, the receptor contains signals for active anterograde transport as well as selective recycling within its short cytosolic C terminus (Foresti et al., 2010). Transport competition assays revealed that the rate-limiting transport step is the recycling from the PVC, which is also wortmannin sensitive (daSilva et al., 2005). VSR transport critically depends on the conserved Tyr-Met-Pro-Leu (YMPL) motif that mediates interaction with clathrin adaptor complexes (Sanderfoot et al., 1998; Happel et al., 2004). Substituting

[1] Current address: Cell and Developmental Biology Programme, Center for Genomic Regulation, Universitat Pompeu Fabra, Barcelona, Spain.
[2] Current address: Faculdade de Medicina de Ribeirão Preto-Universidade de São Paulo, Departamento de Biologia Celular e Molecular, Av. dos Bandeirantes 3900, 14049900-Ribeirão Preto, São Paulo, Brazil.
[3] Current address: Department of Cell Biology, Yale University, School of Medicine, New Haven, CT 06520-8002.
[4] Address correspondence to j.denecke@leeds.ac.uk.
The author responsible for distribution of materials integral to the findings presented in this article in accordance with the policy described in the Instructions for Authors (www.plantcell.org) is: Jurgen Denecke (j.denecke@leeds.ac.uk).
[W] Online version contains Web-only data.
[OPEN] Articles can be viewed online without a subscription.
www.plantcell.org/cgi/doi/10.1105/tpc.113.122226

this Tyr with Ala (Y612A) causes partial receptor mistargeting to the PM (daSilva et al., 2006) and the TGN (Foresti et al., 2010). Mutagenesis of the Leu (L615A) causes defective receptor recycling from the PVC and leakage to a rab5-labeled late prevacuolar compartment (LPVC) and the vacuole, where it is more rapidly degraded (Foresti et al., 2010). There is also evidence to suggest that the conserved ExxxIM motif present in the exposed terminus plays an important role in receptor transport (Saint-Jean et al., 2010). Finally, strong evidence indicates a role for the cytosolic retromer core complex in receptor salvage from the PVC (Kleine-Vehn et al., 2008; Kang et al., 2012).

It has recently been proposed that VSRs may export ligands directly from the ER in a COPII-independent manner, bypassing the Golgi and leading to the TGN, from which they may be recycled back to the ER (Niemes et al., 2010a, 2010b). However, this alternative model is highly controversial, and it has yet to be tested whether the ER export of VSRs is COPII mediated and whether it occurs by bulk flow or via signal-mediated concentration.

Here, we have systematically studied the individual VSR anterograde transport steps in tobacco (*Nicotiana tabacum*) and the protein machinery involved in this process. Evidence is shown to support a model in which VSRs interact with vacuolar cargo in the Golgi apparatus and use the canonical COPII-mediated route to reach it. Rate-limiting VSR transport from the Golgi to the PVC is dependent on a conserved Glu and the well-characterized YMPL motif. Experiments using the entire cytosolic tail demonstrate that wild-type VSRs not only interact with the plant clathrin adaptor AP1 but also with the distantly related AP4 complex that may represent an alternative, possibly clathrin-independent pathway. These machinery components mediate VSR trafficking between the Golgi/TGN and the PVC, specifically avoiding the PM under normal conditions. Endocytic VSR recycling from the PM only takes place in the absence of the YMPL motif and plays no role in canonical cargo delivery to the vacuole.

RESULTS

Soluble Vacuolar Proteins Pass through the Golgi Apparatus

To test if vacuolar proteins pass through the Golgi or reach the TGN in a Golgi-independent manner, we constructed dual-signal cargo molecules exhibiting both the N-terminal aleurain sorting signal for vacuolar transport (Kirsch et al., 1994) and a C-terminal tetrapeptide, His-Asp-Glu-Leu (HDEL), for ER retention (Phillipson et al., 2001). If the aleurain signal causes the cargo to bypass the Golgi stack, HDEL-mediated retrieval is not expected to function, as this occurs from the *cis*-Golgi in plants (Phillipson et al., 2001). If vacuolar sorting occurs from the Golgi cisternae, then the HDEL receptor ERD2 may intercept the fusion protein and sequester it back to the ER. Therefore, we first used a secretory red fluorescent protein (RFP) as cargo and compared the dual-signal cargo (Aleu-RFP-HDEL) with secreted RFP (secRFP), vacuolar RFP (Aleu-RFP), and ER-retained RFP (RFP-HDEL) for fluorescence microscopy in tobacco leaf epidermis cells (Figure 1A).

Figures 1B and 1C show that secRFP is found exclusively in the apoplast and is undetectable in the vacuolar lumen or when in transit through the ER. Addition of the C-terminal HDEL signal prevented apoplastic deposition and caused efficient ER retention under these experimental conditions (RFP-HDEL). As expected from previous findings, the vacuolar fusion Aleu-RFP segregates efficiently from the default secretory route to the vacuole and is found in small punctate structures (Figure 1B) corresponding to LPVC compartments (Foresti et al., 2010) as well as in the central vacuole lumen, where it produces homogeneous fluorescence (Figures 1B and 1C). Interestingly, the dual-signal cargo Aleu-RFP-HDEL was strongly redistributed to the ER, suggesting an efficient retrieval from the Golgi apparatus. Therefore, the aleurain signal for vacuolar sorting does not mediate bypassing of the Golgi apparatus.

Vacuolar Sorting and ER Retention Can Compete with Each Other

Aside from the clear fluorescence of the dual-cargo Aleu-RFP-HDEL in the ER, weak homogeneous fluorescence in the central vacuolar lumen was also seen consistently and was best appreciated at low magnification for cells with the focal plane including the vacuolar lumen (Figure 1C). It was shown previously that HDEL-mediated ER retention can be leaky, possibly via saturation of the sorting receptor ERD2 (Crofts et al., 1999; Pimpl et al., 2006). However, leakage of RFP-HDEL to the apoplast was not detected, suggesting efficient retention of HDEL ligands under these experimental conditions. The weak fluorescence of Aleu-RFP-HDEL in the vacuole, therefore, is unexpected.

To test if a vacuolar sorting signal can compete with an ER retention signal, we repeated the experiment using the barley (*Hordeum vulgare*) α-amylase (Amy) reporter system in tobacco leaf protoplasts (Phillipson et al., 2001), which is more suitable for monitoring secretion quantitatively. Secreted Amy was compared with ER-retained Amy-HDEL (Phillipson et al., 2001), vacuolar Aleu-Amy (Bottanelli et al., 2011), and the test cargo Aleu-Amy-HDEL (Figure 2A). Figure 2B shows that under control conditions, secretion of Aleu-Amy is detected at very low levels, well below the slow secretion of the ER-retained Amy-HDEL and the fast secretion of the control (Amy). The dual-signal cargo Aleu-Amy-HDEL is undetectable in the medium.

To quantify how much of the cargo is exported from the ER and delivered to vacuoles, the drug wortmannin was used, as it specifically redirects vacuolar cargo to the cell surface without affecting the early secretory pathway or constitutive secretion (Pimpl et al., 2003). Therefore, transfected protoplast suspensions were divided into two equal portions, one to be incubated without the drug, giving rise to the data described above (first four lanes of Figure 2B), and the other supplemented with wortmannin, to generate the data in the last four lanes of Figure 2B. The results confirm that the drug did not affect the behavior of the control cargo Amy and the ER-retained Amy-HDEL. However, secretion to the medium was strongly induced for Aleu-Amy and Aleu-Amy-HDEL (Figure 2B). The wortmannin-induced proportion in the medium is representative of the amount that escaped the ER and would normally have been targeted to the vacuoles in the absence of the drug (Figure 2B, compare lanes 3 and 4 with lanes 7 and 8).

The quantitative assays confirm that HDEL effectively causes retention of Aleu-Amy-HDEL compared with Aleu-Amy, ruling out that the aleurain signal causes bypassing of the Golgi. However, Aleu-Amy-HDEL shows significantly more wortmannin-induced

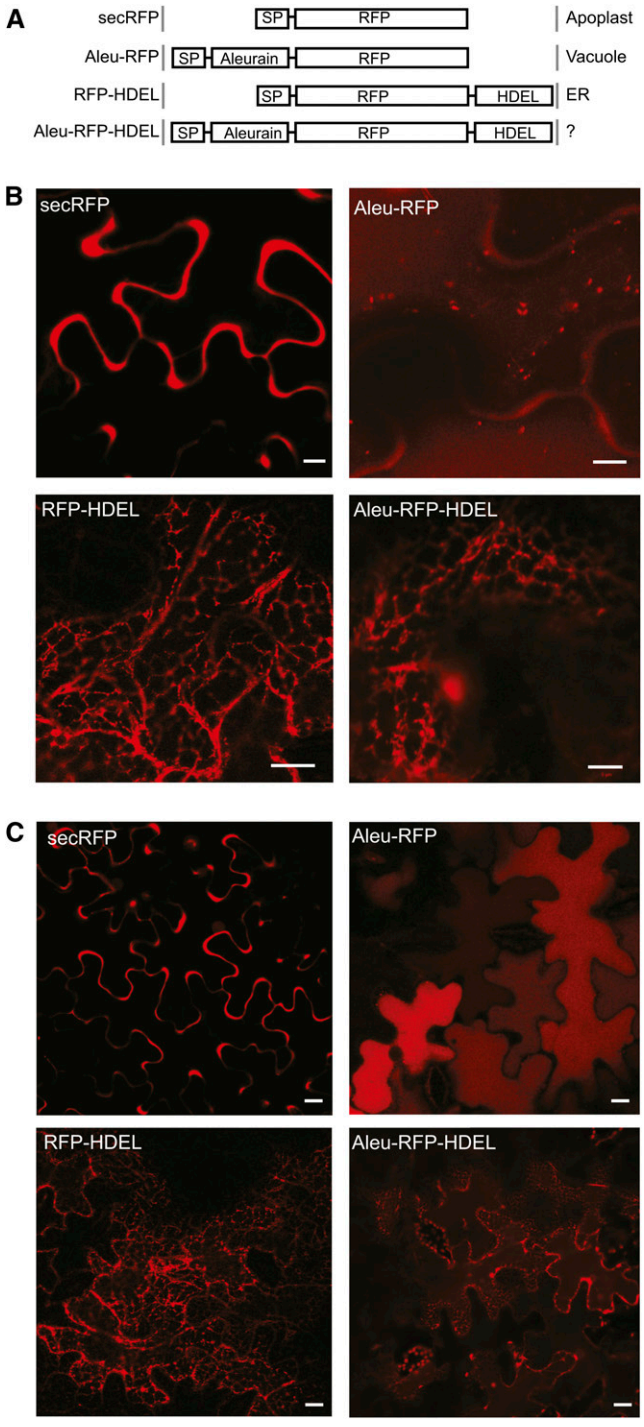

Figure 1. Vacuolar Sorting Does Not Bypass the Golgi Apparatus.

(A) Schematic illustration of the recombinant proteins studied and summary of subcellular localization patterns. SP, signal peptide; Aleurain, propeptide of barley aleurain containing the vacuolar sorting signal.

(B) Confocal laser scanning micrographs of *Agrobacterium*-infiltrated tobacco leaf epidermis cells expressing secRFP, Aleu-RFP, RFP-HDEL, or Aleu-RFP-HDEL. Bars = 5 μm.

(C) As in **(B)**, but micrographs were taken at lower magnification. Bars = 5 μm.

secretion compared with Amy-HDEL, suggesting that the presence of the vacuolar sorting signal reduces the ER retention efficiency. This could be explained if VSRs and ERD2 bind to the dual-signal cargo in a mutually exclusive manner. Competition by the two receptor types is likely to take place on even terms in the Golgi apparatus, because HDEL cargo is established to dissociate from its receptor in the ER (Ceriotti and Colman, 1988; Pelham, 1988; Pelham et al., 1988).

Transport of VSR and Its Cargo Occurs via the Canonical COPII Pathway between the ER and the Golgi

Although we have demonstrated that anterograde VSR transport passes through the Golgi apparatus (Figures 1 and 2), it remains to be shown by which mechanism it leaves the ER. We thus tested if VSRs are exported from the ER in a canonical COPII-dependent pathway using direct transport assays. Overexpressed guanosine nucleotide exchange factor Sec12 titrates the GTPase Sar1 and prevents vesicle budding from the ER (Phillipson et al., 2001). Figure 3A shows that VSR export from the ER and accumulation in the PVC are effectively inhibited by coexpressed Sec12, the presence of which was guaranteed by a Golgi marker within the same T-DNA (Bottanelli et al., 2011). The green fluorescent protein (GFP)-VSR2 fusion was trapped in the ER network, alongside the Golgi marker. This corresponds well with the fact that the ER export of the vacuolar cargo Aleu-RFP is also sensitive to Sec12 overexpression (Bottanelli et al., 2011).

These imaging results could be substantiated by biochemical transport assays in protoplasts in which the progress of GFP-VSR2 through the vacuolar route can be followed by discrete processing steps (daSilva et al., 2005, 2006). Coexpression of increasing quantities of Sec12p led to accumulation of the glycosylated GFP-VSR2 precursor form, which exhibits the highest molecular weight form on the protein gel blots (Figure 3B, pellet). A clear depletion of the lowest molecular weight vacuolar GFP core is also apparent at high Sec12 dosage (Figure 3B, supernatant). COPII-mediated ER-to-Golgi transport can also be inhibited in plants by coexpression with a GTP-restricted mutant form of Sar1 [Sar1(H74L)] that is dominant over endogenous wild-type Sar1 (Takeuchi et al., 2000; Phillipson et al., 2001). Compared with Sec12 overexpression, coexpression of the GTP-restricted Sar1 (H74L) led to a much faster shift from the low molecular weight vacuolar GFP core form to the glycosylated GFP-VSR2 precursor (Figure 3B, compare the last five lanes with the mock lane).

Although the results confirm that VSRs are exported from the ER in a canonical COPII-dependent manner, we wanted to explore the possibility that perhaps a small portion of VSRs reach the Golgi in a COPII-independent manner or even bypass the Golgi. For this purpose, we coexpressed plasmids encoding either GFP-VSR2 or the bulk flow marker Amy in the same protoplast suspension and tested a Sar1(H74L) dose response on the two different cargo molecules simultaneously. Figure 3C shows that both soluble cargo Amy and membrane cargo GFP-VSR2 undergo a dose-dependent inhibition of transport. Amy activity increases in the cells at the expense of Amy activity in the medium, and this shift occurs gradually with each increase in the Sar1(H74L) dosage. In contrast, GFP-VSR2 processing is already

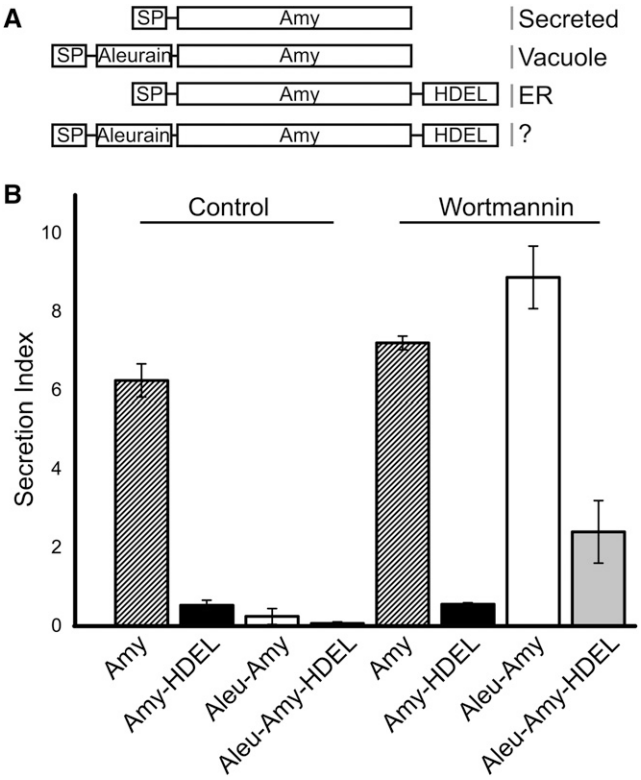

Figure 2. Vacuolar Sorting and ER Retention Mechanisms Compete with Each Other.

(A) Schematic illustration of the recombinant proteins studied and summary of subcellular localization patterns. Annotations are as in Figure 1, but RFP is replaced by Amy.

(B) Transient protein secretion assay in electroporated tobacco leaf protoplasts. Shown is the secretion index (the ratio of extracellular to intracellular α-amylase activity) depending on the type of recombinant protein (Amy, Aleu-Amy, Amy-HDEL, or Aleu-Amy-HDEL) under control conditions or in the presence of wortmannin (33 μM). Error bars indicate SD from five independent transient expression experiments.

maximally affected at the lowest inhibitor dosage, suggesting that the receptor fusion is more sensitive to Sar1(H74L). If a portion of VSRs would bypass the COPII-mediated pathway, the opposite should have been observed.

Combined, the results in Figures 1 to 3 refute the proposal that plant VSRs bypass the Golgi (Niemes et al., 2010a), and we propose that they are exported from the ER using the canonical COPII pathway together with soluble secretory proteins. Segregation of vacuolar from secretory cargo, therefore, must take place in the Golgi apparatus or later in the pathway.

VSR Export from the ER Occurs by Bulk Flow

Previous work on the GFP-VSR2 fusion established that deletion of the cytosolic tail downstream of the positive amino acid cluster near the transmembrane domain (GFP-VSR2ΔCT) led to partial retention in the ER and abolished in vivo competition with endogenous VSRs (daSilva et al., 2006), suggesting a severe transport defect. In order to test the requirements for VSR ER export and post-Golgi trafficking, we decided to compare this deletion construct with a series of shorter deletions up to and including the YMPL motif (Figure 4A).

Figure 4B shows that the longest deletion (GFP-VSR2ΔCT) expressed in tobacco leaf epidermis is mostly present in a typical ER network, in line with earlier observations with the same construct in protoplasts (daSilva et al., 2006). In addition to the ER labeling, mobile punctate structures were also observed, suggesting that a minor portion is exported from the ER. Lengthening the C terminus by nine amino acids (Δ23) strongly promoted ER export, and the resulting fusion protein was found in punctate structures and the PM. The two shortest deletions (Δ19 and Δ15) yielded mainly punctate structures, showing that further sorting information prevented accumulation at the PM, either by decreased transport to or accelerated endocytosis from the cell surface.

To understand why GFP-VSR2-ΔCT is ER retained and GFP-VSR2Δ23 proceeds to the PM, we analyzed specific residues in the membrane-proximal region of the VSR cytosolic tail tide (QYMDSEIRA) that distinguishes between the two constructs. Both DXE (Barlowe et al., 1994; Nishimura and Balch, 1997; Nishimura et al., 1999; Hanton et al., 2005; Chatre et al., 2009) and YXDXE (Sevier et al., 2000) motifs have been demonstrated to be essential for ER export in eukaryotes and are present in this peptide region. We hypothesized that mutations in a putative ER export motif would reduce the ability of full-length VSR tails to compete with endogenous receptors for sorting machinery. For this reason, the in vivo competition assay previously used to identify signals regulating rate-limiting VSR transport steps (daSilva et al., 2005, 2006) was developed further. GFP-VSR constructs were cloned in a dual expression plasmid carrying a gene for cytosolic β-glucuronidase (GUS) as an internal reference for protoplast transfection efficiency (Figure 4C). The GFP-VSR full-length tail construct was used as a positive control and compared with specific point mutations and combinations covering the putative YXDXE motif. These included the single mutations Y600A, D602A, and E604A as well as the combination of the two acidic residues, DE602/604AA (DE), or all three candidate residues, YDE600/602/604AAA (YDE).

After establishing the conditions for comparable transfection efficiencies using the GUS reporter, the dual-expression plasmids were used for dose–response assays and cotransfected at increasing levels with a constant amount of vacuolar cargo amy-spo–encoding plasmid. GUS was measured again in all samples to establish the dose as well as the amylase activity in the medium and in the cells to monitor the response. The resulting amy-spo secretion index (the ratio of activity in the medium to that in the cells) was then plotted as a function of the corresponding internal GUS level to reveal the dose–response analysis. The resulting slope (Figure 4D) was calculated from the individual scatterplots (Figure 4E). The results show that the conserved residues Tyr-600 and Asp-602 were not required for in vivo competition, as they exhibited almost wild-type-like competition. By sharp contrast, Glu-604 appeared to be critically required for in vivo competition, and the dose response was not affected much further when combined with one or both of the other mutations (DE and YDE) (Figure 4D).

Next, we wanted to establish if mutation of the DXE sequence resulted in ER retention of the GFP-VSR fusion. Thus, the

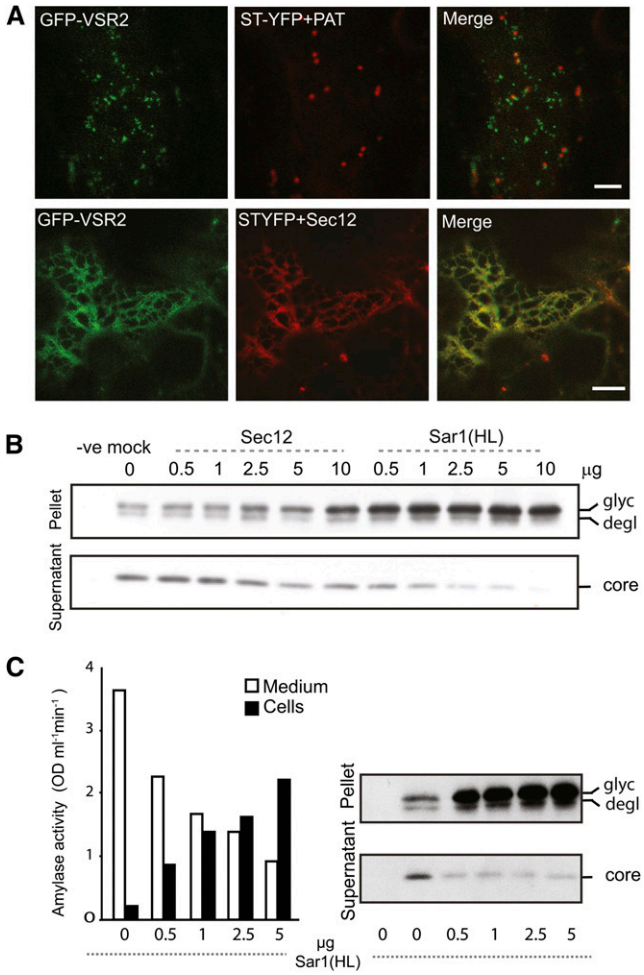

Figure 3. VSR Transport from the ER to the Golgi Is COPII Mediated.

(A) Confocal laser scanning micrographs of *Agrobacterium*-infiltrated tobacco leaf epidermis cells coexpressing the fluorescent receptor model cargo GFP-VSR2 with either a dual construct encoding a yellow fluorescent Golgi marker (ST-YFP) with the mock effector cytosolic phosphinothricin acetyl transferase (PAT) or a dual construct combining ST-YFP with a Sec12 overexpression construct known to inhibit ER export in plants (Phillipson et al., 2001). The cells were imaged at the cell cortex and are shown in three-channel mode (green, red, and merged in yellow). Note that both GFP-VSR2 and the Golgi marker ST-YFP redistribute to the ER network in the presence of Sec12 overexpression. Bars = 5 μm.

(B) Transient expression experiment in tobacco leaf protoplasts. Protein gel blots show the inhibition of intracellular GFP-VSR2 processing to the vacuolar GFP core (core) as a function of the COPII transport inhibitors Sec12 and Sar1(H74). Transfected effector plasmid concentrations are indicated in micrograms above each lane. GFP-VSR2–encoding plasmid was electroporated using a constant amount of 20 μg in each sample. Membrane-spanning GFP-VSR2 precursors are in the pellet fraction containing the glycosylated (glyc) and deglycosylated (degl) forms, as in daSilva et al. (2006).

(C) Transient expression experiment in tobacco leaf protoplasts, illustrating that GFP-VSR2 processing is more sensitive to Sar1(H74L) coexpression than constitutive secretion of soluble proteins. A mixture of GFP-VSR2– and α-amylase–encoding plasmids (20 μg each) was coexpressed with a dilution series of plasmid encoding Sar1(H74L), with plasmid quantities of the dilution series indicated under each lane in micrograms. Secreted Amy is recovered from the culture medium, while extraction of soluble proteins from cells yields Amy in transit and the vacuolar GFP core found in the vacuole (daSilva et al., 2005). Further extraction of the cell pellet with detergents solubilizes the membrane-spanning fusion protein GFP-VSR, showing the glycosylated precursor in transit through the ER/Golgi and a deglycosylated form in transit through the Golgi-PVC pathway to the vacuole (daSilva et al., 2006). Annotations of GFP-VSR2 processing forms are as in **(B)**.

subcellular fluorescence pattern of GFP-VSR2 was compared with that of the corresponding DE mutant. Figure 5A shows that the mutant is exclusively found in punctate structures, similar to the pattern of the wild-type fusion. There was no evidence for an extensive ER network, suggesting that the DE double mutant is fully ER export competent. This result suggests that, despite exhibiting a DXE consensus signature, the sequence plays no role in ER export.

To test if ER retention of GFP-VSR2-ΔCT is due to the absence of an active sorting signal or to inadvertent exposure of basic amino acids near the new C terminus, we decided to test the effect of fusing the random pentapeptide sequence NFLET (Figure 5B) to replace the original QYMDS sequence at this position. The ΔCT and ΔCT-NFLET constructs were compared by compiling individual images from Z-stacks into a single maximum intensity projection (Figure 5C) using methodology described previously (Kural et al., 2012). The results revealed that addition of this pentapeptide strongly enhanced the ER export properties, causing a dramatic shift from the highly intense ER network pattern of ΔCT (Figure 5D) to the typical diffuse fluorescence of the PM and small punctate structures (Figure 5E), similar to GFP-VSR2Δ23 (Figure 4B). These results suggest that VSRs are exported from the ER by COPII-mediated bulk flow, without the need for any specific export signals.

The VSR Tail Interacts with the Plant Clathrin Adaptor Complex AP1 and the Adaptor Complex AP4

If VSR export from the ER does not require signals, post-ER segregation of VSRs to the vacuolar route must be signal mediated. Previous studies implementing the cytosolic medium subunit of adaptor protein complexes (muAPs) for clathrin-mediated VSR cargo transport are controversial. One study showed a binding preference for mammalian muAP1 rather than mammalian muAP2 (Sanderfoot et al., 1998), suggesting a main role of TGN-derived CCVs in anterograde VSR transport. A later study suggested that *Arabidopsis thaliana* muAP2 interacts with the YMPL motif of plant VSRs (Happel et al., 2004), implying that CCVs carrying VSRs (Kirsch et al., 1994) may be of endocytic origin instead. To distinguish between these two possibilities, we cloned the entire cytosolic tail of VSR2 in the yeast two-hybrid vector pBridge as bait to fully appraise the binding capabilities within the native sequence context, which was shown to contribute to specificity (Ohno et al., 1996; Kirchhausen et al., 1997; Rapoport et al., 1998). As prey, mammalian μ-subunits of AP1A, AP1B, AP2, AP3A, and AP4 were expressed fused to the Gal4AD in the yeast two-hybrid vector pACT2 (Ohno et al., 1999; Guo et al., 2013). We also cloned

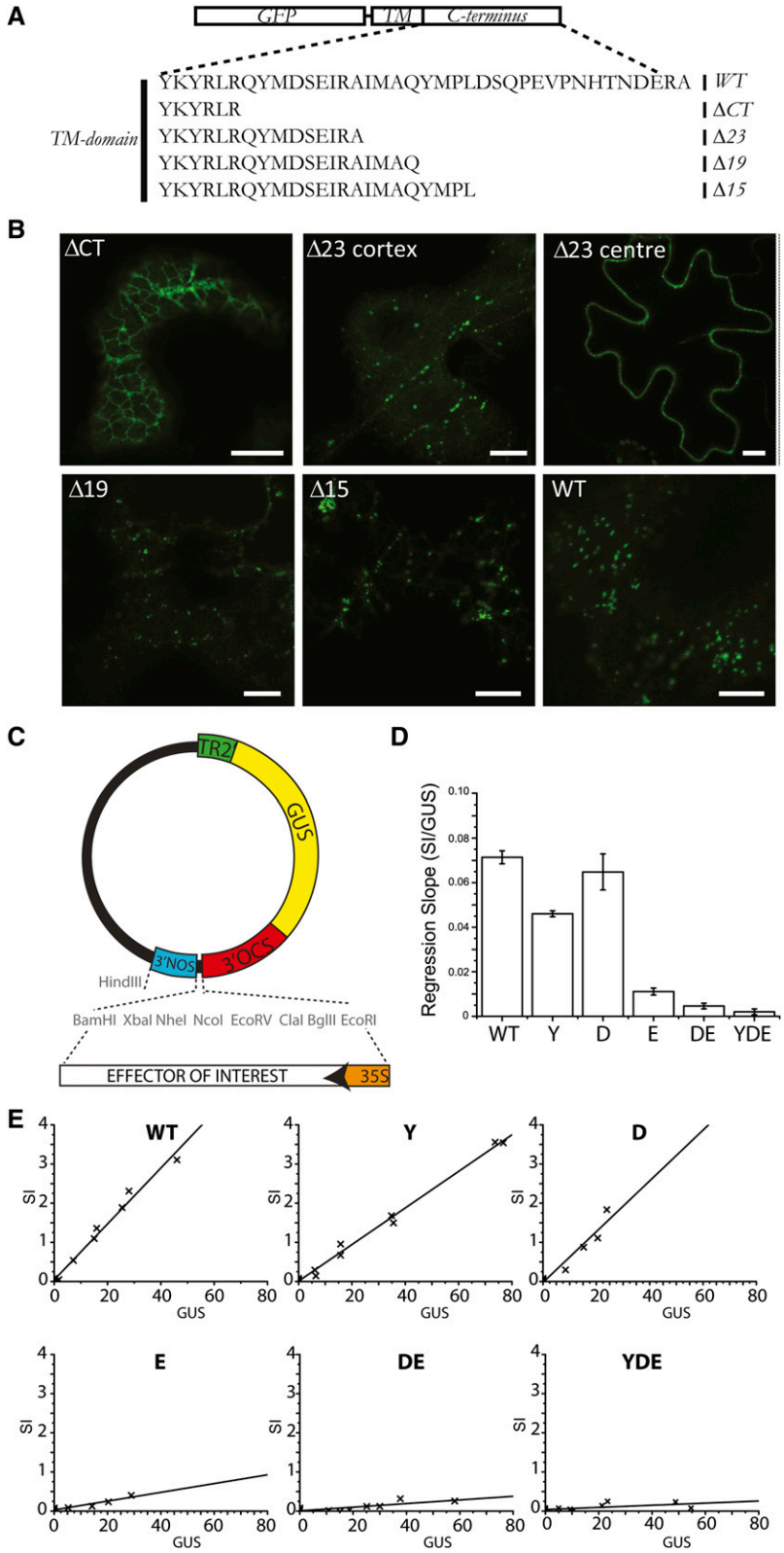

Figure 4. Subcellular Localization Analysis of VSR2 Deletion Mutants.

cDNAs encoding *Arabidopsis* μ-subunits of AP1A, AP1B, AP2, AP3, and AP4, the identity of which is readily identified phylogenetically, and inserted these into the same pGADT7 vector to repeat the interaction studies.

Figure 6A shows that the cytosolic tail of VSR2 interacts with mammalian muAP1A but not muAP1B, muAP2, muAP3A, or muAP4. Instead, the cytosolic tail of mammalian TGN38 (Ohno et al., 1996) interacts with muAP1A, muAP2, and muAP3A but not muAP1B or muAP4. Interestingly, the two tails interact differentially with the *Arabidopsis* muAPs (Figure 6B). While the plant VSR2 tail interacts with *Arabidopsis* muAP1A, muAP1B, and muAP4 but not muAP2 or muAP3, TGN38 interacts with all the *Arabidopsis* μ-subunits, but most weakly with muAP1A and muAP1B. A role of plant AP4 complexes in plant vacuolar sorting is not documented and may explain why the inhibition of clathrin-mediated protein sorting fails to disrupt biosynthetic vacuolar sorting (Scheuring et al., 2011; Hirst et al., 2012, 2013).

The VSR C Terminus Regulates Distinct Transport Steps to and from the PVC

It is shown above that two separate adaptor complexes may mediate selective VSR transport from the Golgi apparatus and beyond. To test if this unexpected complexity is reflected by multiple transport pathways, we wanted to determine the subcellular fate of the previously generated VSR C-terminal deletions (Figure 4A). While ER and PM can be identified morphologically, analyzing the identity of the punctate organelles required systematic coexpression of the four GFP-VSR2 deletion constructs with the Golgi marker ST-RFP, the TGN marker RFP-SYP61, or the PVC marker RFP-VSR2. In contrast to GFP-VSR2 and the well-defined YMPL mutants (Foresti et al., 2010), none of the new deletions shows a clear colocalization with just one of the organelle markers. Instead, colocalization was partial at best, although trends could be established after extensive correlation analysis from large data sets (at least 400 punctate structures for each combination) using the PSC colocalization plugin for ImageJ (French et al., 2008) to calculate Spearman correlation coefficients and red–green scatterplots (Figure 7).

The post-ER signals observed for GFP-VSR2-ΔCT were best correlated with the Golgi bodies, followed by the PVC and only a very weak correlation with the TGN. Taken together with the results in Figure 4B, the distribution trend of ΔCT was thus ER > Golgi > PVC > TGN. The next shorter deletion (GFP-VSR2Δ23) resides predominantly in the PM rather than the ER and shows a clear shift toward the TGN as the main punctate organelle of residence. This gives rise to a totally different steady state distribution for Δ23: PM > TGN > PVC > Golgi. Finally, the two shortest deletions (Δ19 and Δ15) were mainly found at the PVC, with little in transit through the two earlier compartments and no labeling of the ER and the PM.

Evidence for YXXϕ-Independent VSR Targeting to the PVC

The region that differentiates Δ23 and Δ19 contains a highly conserved IM motif present in all plant VSRs (De Marcos Lousa et al., 2012), previously implicated in endocytosis from the PM and recycling from the PVC (Saint-Jean et al., 2010). To test this construct within our model system, we generated the point mutations I608A and M609A on the standard VSR fusion, termed GFP-VSR2 (IMAA), as well as within the remit of the Y612A mutation (IMAA +Y612A), and tested the subcellular localization in tobacco leaf epidermis cells. We observed that the IMAA mutation alone does not change the distribution in comparison with GFP-VSR2 (Figure 8A). In contrast, the same mutation causes a dramatic redistribution to the PM when imposed onto the Y612A mutant (IMAA+Y612A). Therefore, our results here suggest a crucial role of the IM motif in preventing PM accumulation when the YMPL motif is absent (compare with Δ23 with Δ19 in Figure 4C) or mutated (IMAA+Y612A) (Figure 5E). However, this does not show if the IM motif prevents arrival at the PM or allows increased endocytosis.

To further describe potential differences in the route to the PVC taken by Δ19 and Δ15, we performed an additional test to monitor leakage to the LPVC. We expressed the LPVC marker RFP-Rha1 under the transcriptional control of the weak pNOS promoter (Teeri et al., 1989) to avoid merging of PVC and LPVC markers (Bottanelli et al., 2012). Upon coexpression with either GFP-VSR2Δ19 or GFP-VSR2Δ15, we tested potential colocalization with the LPVC (Figure 8B). The Δ19 construct shows a much better colocalization with RFP-Rha1 compared with the Δ15 construct, which contains the YMPL motif and is expected to recycle from the PVC (Foresti et al., 2010). While no distinct red-only LPVC structures could be discerned for the Δ19 mutant, the

Figure 4. (continued).

(A) Schematic view of the VSR C terminus and the deletions used in this study. TM, transmembrane.

(B) Confocal laser scanning micrographs of *Agrobacterium*-infiltrated tobacco leaf epidermis cells expressing four deletion mutants of the fluorescent receptor model cargo GFP-VSR2. Shown is the cortex of a cell expressing the deletion ΔCT, Δ23, Δ19, or Δ15. To appreciate the partial PM partitioning of the Δ23 mutant, two images are shown, with the focal plane either at the cortex or the center of the cell. All other images are taken with the focal plane at the cortex to visualize ER and punctate organelles. Bars = 5 μm.

(C) Schematic of the dual-expression vector containing the internal marker GUS for the normalization of transfection efficiencies. This vector has been used to insert coding regions for GFP-VSR2wt and a series of point mutations, including Y600A, D602A, E604A, DE602/604A, and YDE600/602/604AAA.

(D) Overview of the observed slopes from the individual dose–response assays for each construct, showing the inhibition of vacuolar sorting as a function of the internal GUS reference. Error bars represent SE of the distance of all data points from the individual calculated slopes in **(E)**.

(E) Individual X/Y scatter graphs illustrating individual secretion index (SI) data points plotted as a function of internal GUS reference activity (relative GUS activity) and linear regression lines.

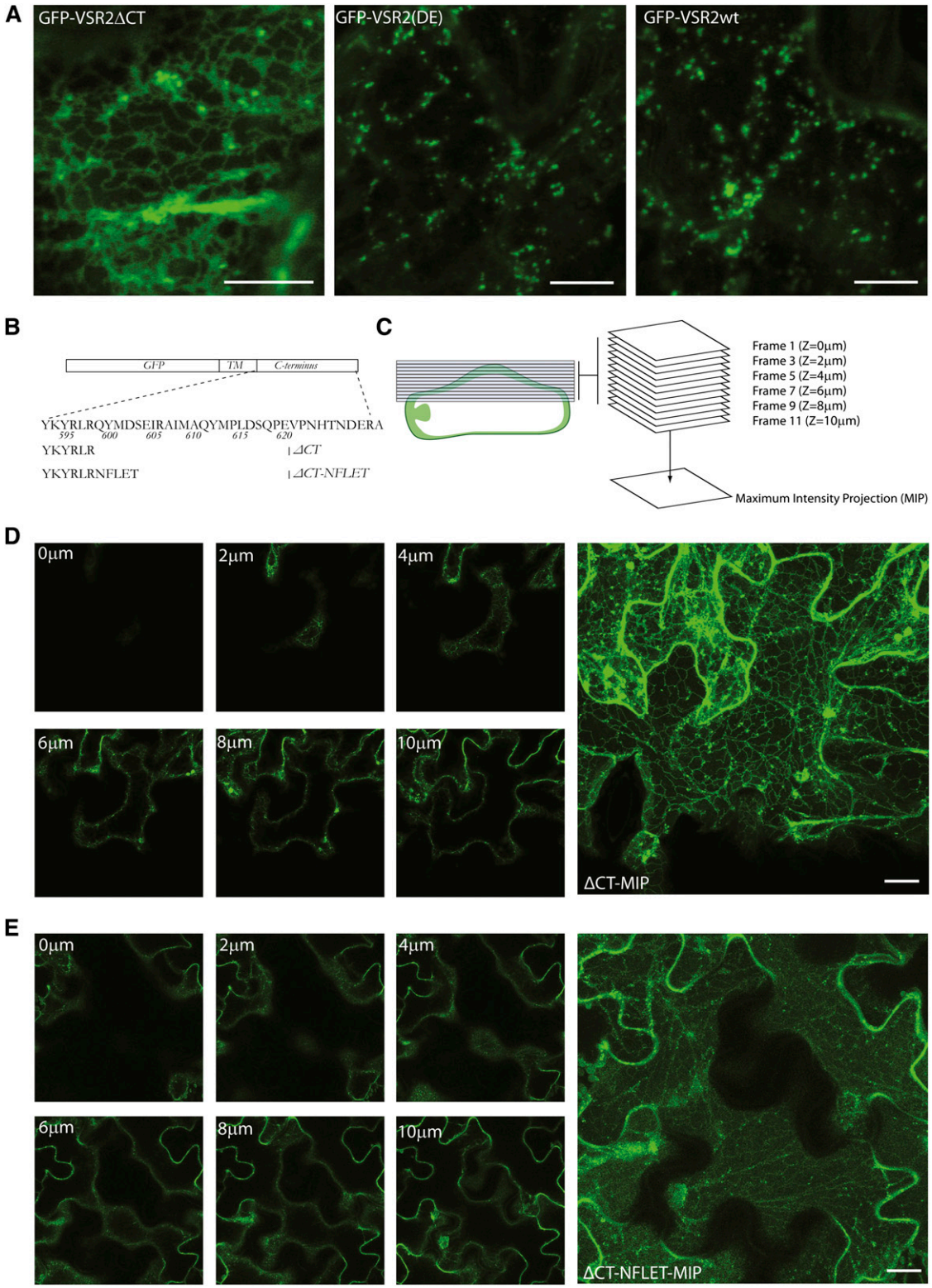

Figure 5. Analysis of the VSR ER Export Dependence.

(A) Confocal laser scanning micrographs of *Agrobacterium*-infiltrated tobacco leaf epidermis cells expressing GFP-VSR2ΔCT, wild-type GFP-VSR2, or the point mutant (DE). Bars = 5 μm.

GFP-VSR2Δ15 panel contains specific red-only LPVC punctae that represent segregating LPVCs (Figure 8B, white arrowheads).

In order to obtain statistically meaningful data, we performed a correlation analysis using the same statistical rigor as employed in Figure 7A, but extending the analysis by a segmented population analysis of scatterplots shown to reveal population shifts in colocalization experiments (Bottanelli et al., 2012). Scatterplots were subdivided into 16 pie segments of equal surface, representing data bins of 16 different categories with progressively increasing red:green ratios (from left to right). Figure 8C illustrates that GFP-VSR2Δ15 segregates from the LPVC marker, as seen by a sharp increase in the height of the red bars on the right side of the bar charts. This is consistent with the presence of a YMPL motif, which reduces leakage of GFP-VSR2Δ15 to the LPVC. In contrast, GFP-VSR2Δ19 colocalizes better with RFP-Rha1, and the scatterplot does not reveal a specific red-only population, similar to earlier observations with the recycling-defective GFP-VSR2 (L615A) mutant (Foresti et al., 2010). Therefore, YXXϕ-independent PVC targeting of the Δ19 mutant results in a recycling-defective phenotype.

The IM Motif Mediates Endocytosis from the PM

Figures 4 and 7 show that GFP-VSR2Δ23 is found at the TGN and PM, and introduction of the IMAQ tetrapeptide (termed Δ19) causes the resulting fusion to accumulate at the PVC/LPVC instead. This shift in steady state can either be due to increased endocytosis or reduced exocytosis of the fluorescent Δ19 mutant. Earlier indications regarding a potential role of the conserved IM motif in endocytosis (Saint-Jean et al., 2010) can equally be explained by IM-mediated TGN-to-PVC transport. To clarify the role of the IM motif and to specifically interrogate potential receptor transit via the PM, we used the ligand binding and release properties of the full-length receptor. Imposing the Y612A mutation on full-length VSR2 causes the mutant receptor to be mistargeted to the PM, during which it "drags" cargo away from endogenous receptors by competition and "drops" it off for secretion instead (daSilva et al., 2006; Foresti et al., 2010). Here, we generated the four truncations (Figure 9A) on the full-length receptor (flVSR2) to test which of the resulting mutants transit via the PM, causing the drag-and-drop activity monitored by increased amy-spo secretion.

The four flVSR2 deletion mutants, as well as flVSR2 wild type and its dominant-negative flVSR2(Y612A) mutant as negative and positive controls, respectively, were inserted into the GUS dual-expression plasmid used above and coexpressed as a dilution series with constant amounts of plasmids encoding vacuolar cargo amy-spo. Following gene transfer and incubation, the measured amy-spo secretion index (the ratio of activity in the medium to that in the cells) was plotted as a function of internal GUS standards, resulting in a dose–response analysis (Figures 9B and 9C).

Overexpressed wild-type flVSR2 shows only minor effects on the cargo and serves as a baseline for the experiments. flVSR2 (Y612A) causes dose-dependent induced secretion of vacuolar cargo, as expected (daSilva et al., 2006; Foresti et al., 2010). Interestingly, complete deletion of the cytosolic tail (flVSR2ΔCT) results in a 4-fold increased amy-spo secretion compared with the wild-type baseline, not much below the increase observed for the Y612A mutant (Figures 9B and 9C). This suggests that VSR–ligand interactions in the ER are infrequent or nonexistent and that small quantities of flVSR2ΔCT reaching the PM by bulk flow can cosecrete ligands efficiently. Addition of the sequence QYMDSEIRA (flVSR2Δ23) shows a further increase in vacuolar cargo secretion compared with flVSR2ΔCT, exhibiting a steeper dose response (Figures 9B and 9C). This is consistent with a faster ER exit of the Δ23 mutant, probably by a lack of C-terminal exposure of basic amino acids that could cause ER retention of the ΔCT construct (Figure 4B).

Interestingly, further inclusion of the tetrapeptide IMAQ (Δ19) results in a receptor molecule that mediates the strongest induction of amy-spo secretion, showing the steepest dose response compared with the positive control flVSR2(Y612A) and flVSR2Δ23 (Figures 9B and 9C). This shows that the addition of the IMAQ peptide does not prevent PM arrival but instead promotes endocytosis. Continuous cycling between the PM and the early secretory pathway may explain why the Δ19 constructs exhibit the highest drag-and-drop activity.

Finally, inclusion of the YMPL motif in the shortest deletion (Δ15) drastically reduces the dose-dependent cargo secretion to the lowest levels of all mutants tested. The dose response of Δ15 is even lower than that of ΔCT, illustrating the strong impact of the YMPL motif in preventing PM arrival. This corresponds well with the binding to AP1, generally localized to the Golgi/TGN, but not AP2, thought to mediate endocytosis (Figure 6). The fact that it does not act identically to the wild-type VSR can be explained by partial functionality of the YMPL without the spatial context of the complete tail (Ohno et al., 1996; Kirchhausen et al., 1997; Rapoport et al., 1998).

The YMPL Motif Is Dominant and Actively Prevents Ligand Loss to the Apoplast

We have shown above that VSRs can endocytose when they reach the PM but are unlikely to do so when a functional YMPL motif is present. We next wanted to test if YMPL-mediated transport to the PVC can actively override the well-documented effect of long transmembrane domains in promoting PM accumulation (Brandizzi et al., 2002). Two further receptor mutants

Figure 5. (continued).

(B) Schematic of the VSR2 consensus C terminus, the VSR2 ΔCT, and the ΔCT-NFLET used in this study. TM, transmembrane.

(C) Diagram illustrating the principle of generating maximum intensity projections (MIP) from a Z-stack.

(D) Selected images from a Z-stack of a tobacco epidermis cell expressing GFP-VSR2ΔCT and a maximum intensity projection assembled from a minimum of 20 individual 1-μm slices. Bar = 5 μm.

(E) As in **(D)**, but from a cell expressing GFP-VSR2ΔCT-NFLET. Bar = 5 μm.

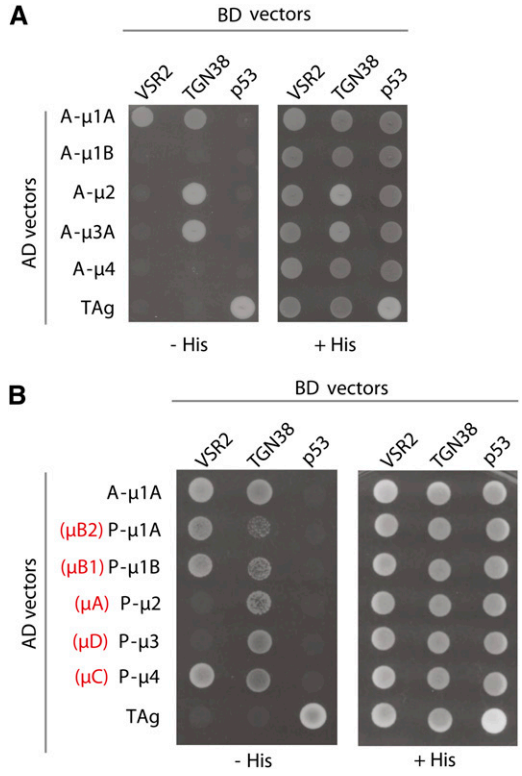

Figure 6. Differential Recognition of VSR2 and TGN38 Cytosolic Tails by μ-Subunits of Mammalian and Plant (*Arabidopsis*) AP Complexes.

(A) *Saccharomyces cerevisiae* strain AH-109 cells were cotransformed with combinations of plasmids encoding Gal4BD fused to the cytosolic tail of VSR2 or TGN38 (indicated on the top of each lane) and plasmids encoding Gal4AD fused to animal (A-) μ-subunits mu1A, mu1B, mu2, mu3A, or mu4 (indicated on the left). Double transformants were plated in medium lacking Leu, Trp, and His (−HIS) to detect interaction among the proteins or in medium lacking Leu and Trp (+HIS) as a control for the loading and viability of the double transformants. As a positive control for interaction, yeast cells were transformed with vectors encoding AD and BD fusions to SV40 large T antigen (TAg) and mouse p53, respectively. Yeast cells were also transformed with a combination of BD-VSR2CT or BD-TGN38CT plasmids with AD-TAg plasmid as a control for self-activation of the cytosolic tail constructs.
(B) Yeast cells were cotransfected with plasmids encoding Gal4BD fused to the cytosolic tail of VSR2 or TGN38 and plasmids encoding Gal4AD fused to mammalian mu1A (A-mu1A) or *Arabidopsis* plant (P-) μ-subunits mu1A, mu1B, mu2, mu3, or mu4 (indicated on the left) and plated on the selective medium described in **(A)**. An alternative nomenclature previously used for *Arabidopsis* μ-subunits is indicated in red.

were thus created by elongating the VSR2 transmembrane domain by four hydrophobic amino acids, followed either by a wild-type cytosolic tail or the Y612A transport mutant. Figure 10A shows the subcellular locations of the two long transmembrane domain (LO) constructs GFP-VSR2LO and GFP-VSR2LO(Y612A) in comparison with GFP-VSR2 and GFP-VSR2(Y612A). Expression in tobacco leaf epidermis cells (Figure 10A, top row) reveals that lengthening of the transmembrane domain alone can lead to a similar partial PM partitioning, as observed previously by introducing the Y612A point mutation. Combining the two modifications resulted in an almost exclusive localization of GFP-VSR2LO(Y612A) to the PM. This is best appreciated by imaging protoplasts prepared from transgenic leaf epidermis cells and imaged at the center of the cell so that the PM forms a sharp uninterrupted smooth circle around the cell (Figure 10A, bottom row).

Using this information on PM partitioning, we repeated the drag-and-drop assay by creating combinations of long transmembrane domains (LO) with or without the Y612A substitution within the context of the full-length receptor, yielding the constructs flVSR2LO and flVSR2LO(Y612A). These were subject to the same GUS-normalized dose–response assays to monitor the induced amy-spo secretion as in Figure 9. Figure 10B shows that lengthening the transmembrane domain alone yielded little or no effect on amy-spo secretion compared with the wild-type construct. This confirms that the presence of a fully functional YMPL motif within its native context of the cytosolic tail effectively prevents PM arrival.

The two constructs harboring the Y612A mutation yielded a strong dose-dependent amy-spo secretion, regardless of the size of the transmembrane domain. Therefore, the absence of a functional YMPL motif enables the drag-and-drop effect, while further repartitioning from the TGN to the PM in the double mutant (LO+Y612A) did not exacerbate induced amy-spo secretion. This was confirmed after creating a mutant full-length receptor bearing the IMAA mutation as well as the Y612A substitution [flVSR2(IMAA +Y612A)]. Although this double mutant effectively accumulates at the PM (Figure 8A) (see also Saint-Jean et al., 2010), similar to the combination of the long transmembrane domain with the Y612A mutant (Figure 10A), it does not induce amy-spo secretion more than the control construct flVSR2(Y612A).

These results are consistent with the idea that both the IMAA mutation and lengthening the transmembrane domain inhibit endocytosis from the PM rather than promote targeting to the cell surface. In mammalian cells, it has been suggested that exclusion of membrane proteins with long transmembrane domains from clathrin-coated pits explains higher steady state levels at the PM (Mercanti et al., 2010). If the rate of exocytosis is unaffected, it would explain why the proteins yield a higher steady state level at the PM without mediating a more pronounced drag-and-drop missorting of vacuolar cargo.

DISCUSSION

Evidence for COPII-Mediated ER-to-Golgi Transport of Plant VSRs

It has been suggested that VSRs select ligands in the ER and progress to the TGN using a novel COPII-independent manner, bypassing the Golgi apparatus (Niemes et al., 2010a). This is in contrast with evidence for VSR transit through the Golgi apparatus based on glycan modification studies (daSilva et al., 2006; Kim et al., 2010) and immunocytochemistry (Hinz et al., 1999), but those studies could not distinguish between arrival at the Golgi in an anterograde or retrograde manner. To test if VSRs use a COPII-independent ER-to-Golgi pathway, we used inhibitors of the COPII-mediated pathway that have been characterized previously (Takeuchi et al., 2000; Phillipson et al., 2001). Both Sec12 overexpression as well as Sar1(H74L) coexpression inhibited GFP-VSR2 export from the ER (Figure 3). These results also indicate that the Golgi apparatus is the next step in the anterograde VSR transport,

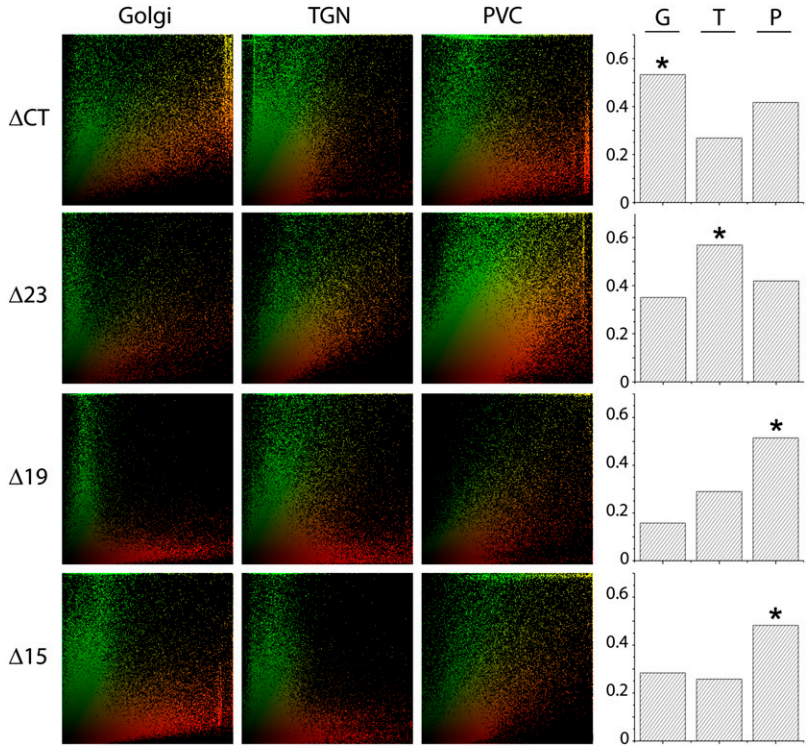

Figure 7. Subcellular Distribution of GFP-VSR2 Deletion Mutants in Punctate Structures.

Statistical correlation analysis of GFP-VSR2 ΔCT, Δ23, Δ19, or Δ15 was performed with the Golgi marker ST-RFP, the TGN marker RFP-SYP61, or the PVC marker RFP-VSR2. The scatterplots are representative of at least 400 punctate structures, comprising a minimum of 50,000 pixels. On the right, the Spearman correlation coefficients are shown (G, Golgi; T, TGN; P, PVC) for each deletion construct. The highest correlation is indicated by a star.

because COPII-mediated transport leads to the *cis*-Golgi in plants (Brandizzi and Barlowe, 2013).

Using a dual-signal cargo bearing a vacuolar sorting signal (Aleu) as well as an ER retention signal (HDEL), we could demonstrate a central role of the Golgi apparatus to host interactions between soluble cargo and their receptors (Figures 1 and 2). ER retention occurs via receptor-mediated capture at the Golgi, followed by recycling to the ER and ligand release (Ceriotti and Colman, 1988; Pelham, 1988; Pelham et al., 1988). In plants, HDEL-mediated protein retrieval occurs mainly at the *cis*-Golgi (Phillipson et al., 2001). According to the newly proposed model (Niemes et al., 2010a), the dual-signal test cargo would be captured earlier and bypass the opportunity for recycling. This was not observed in our study. Second, VSR–ligand interactions cannot be restricted to the TGN or late Golgi cisternae either, because in that case HDEL-mediated retrieval from the *cis*-Golgi would have prevailed. Again, such dominant behavior was not observed. The intermediate behavior of the dual-signal cargo suggests that there is equal competition between ERD2 and VSRs and points to the Golgi stack for both types of receptor–ligand interactions, starting at the *cis*-Golgi.

Post-ER Targeting of Plant VSRs Depends on the Adaptor Complexes AP1 and AP4

Having established that VSR trafficking is initiated by COPII-mediated transport to the Golgi, the question remains how it is specifically segregated to the vacuolar transport route. Results from the deletion analysis and addition of the random pentapeptide NFLET to the C terminus of the ER-retained GFP-VSR2ΔCT construct strongly suggest that ER export is not due to specific signals but occurs via bulk flow (Figure 5). Although plant VSR C termini invariantly contain a conserved DXE motif, it seems to play no role in ER export, while Glu-604 appears to be required for the proper functioning of YMPL-mediated receptor trafficking. This illustrates why the structural context of YXXϕ motifs must be considered to fully appreciate the binding specificity to adaptor complexes (Ohno et al., 1996; Kirchhausen et al., 1997; Rapoport et al., 1998).

Using the entire C terminus of VSR2 as bait in a yeast two-hybrid analysis and comparing μ-subunits of AP1, AP2, AP3, and AP4 from mammals and plants, we have specifically demonstrated that VSR tails preferentially interact with muAP1 but not with muAP2 (Figures 6A and 6B). This indicates that VSRs present in isolated plant CCVs (Kirsch et al., 1994; Hinz et al., 1999; Sauer et al., 2013) are derived from Golgi/TGN membranes, the site of action for AP1 complexes (Park et al., 2013). The lack of interaction between the VSR tail and PM-specific AP2 argues against the recently suggested endocytic origin of VSR-containing CCVs (Scheuring et al., 2011).

Interestingly, the experiments also indicated a strong interaction between the VSR tail and muAP4 (Figure 6B). It has recently been shown that AP4-mediated transport may act as

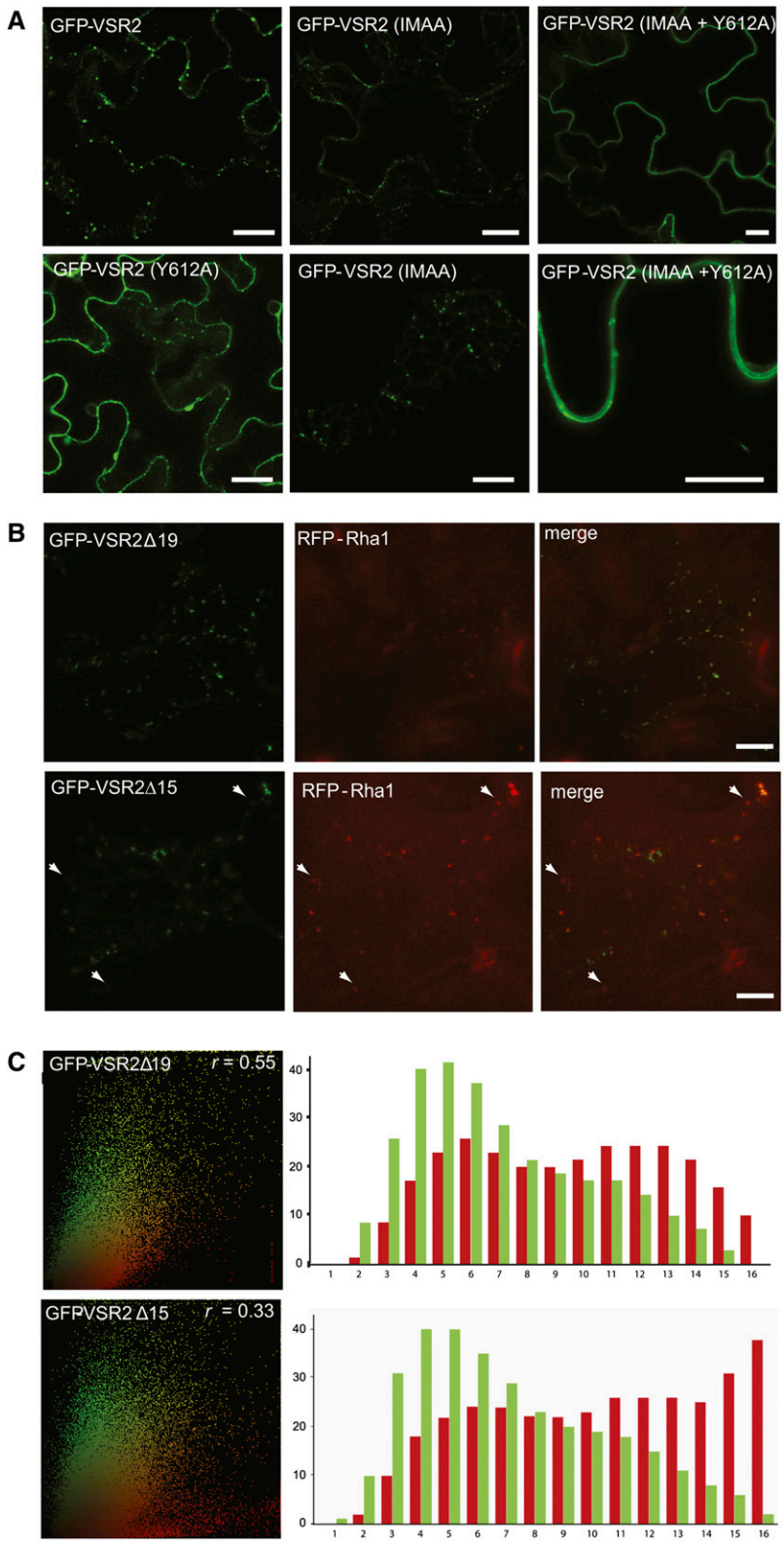

Figure 8. Subcellular Localization of VSR2 Mutants.

a backup route for the AP1-mediated CCV pathway to the mammalian lysosome (Hirst et al., 2012, 2013). If this mechanism is conserved in plants, it would explain why inhibition of the CCV route does not stop biosynthetic vacuolar sorting in plants (Scheuring et al., 2011). Recent experiments in mammalian cells suggest that AP1 could be present in two separate classes of CCVs, one for anterograde and one for retrograde trafficking (Hirst et al., 2012). This is consistent with the discovery that the YMPL motif signals both anterograde and retrograde transport (Foresti et al., 2010), and it would also explain why VSRs were so readily purified from CCVs (Kirsch et al., 1994).

Where Is the Default Location for Type 1 Membrane-Spanning Proteins?

The detailed comparison of GFP-VSR2 fusions with small variations in the cytosolic tail as independent variables (Figures 4, 5, and 7) is ideally suited to study the default location for membrane-spanning proteins in plants. Earlier studies pointed either to the PM (Benghezal et al., 2000) or the tonoplast (Barrieu and Chrispeels, 1999) as the default location. In yeast, removal of the cytosolic tail of the VSR (VPS10) results in accelerated degradation in the vacuole (Cereghino et al., 1995; Cooper and Stevens, 1996). The YXXϕ motif of VPS10, therefore, has been proposed to mediate retromer-dependent receptor recycling from the PVC to the Golgi (Seaman et al., 1997), but in plants, the YXXϕ motif is important for both anterograde and retrograde VSR transport (Foresti et al., 2010), and deletion of the tail (GFP-VSR2ΔCT) leads to significant ER retention (daSilva et al., 2006).

Here, we confirm that GFP-VSR2ΔCT accumulates in the ER, but it can also be detected in the Golgi, the TGN, and the PVC (Figure 7). Shorter deletions of the VSR tail led to high steady state levels either at the PM (GFP-VSR2Δ23 and GFP-VSR2-NFLET) or the PVC/LPVC (GFP-VSR2Δ19), even in the absence of the YMPL motif (Figures 4, 5, and 7). Although specific sorting signals can alter the steady state distribution, it is important to stress that all deletions showed at least partial colocalization with the PVC. We suggest that the lack of a recycling signal for retrieval from the PVC exacerbates leakage to the vacuole, which explains residual processing of the ER-retained GFP-VSR2ΔCT to the vacuolar core fragment (daSilva et al., 2006). However, this occurs via an alternative pathway, as it does not compete with YMPL-mediated trafficking.

It is clear that identification of the highest steady state levels in fluorescence microscopy is insufficient to determine the default location of a membrane protein. Likewise, transit through an organelle may occur in spite of undetectable levels at this compartment. Proteins may accumulate at the ER or the PM, but they will also slowly partition to the vacuole for degradation.

The Drag-and-Drop Assay Reveals Receptor Transit via the PM and Distinguishes Increased Endocytosis from Inhibited Exocytosis

To address these issues, we have expanded the number of tools at our disposal by supplementing fluorescence microscopy with a sensitive biochemical transport assay that actively explores the ligand binding and release properties of the VSR lumenal domain. Although PM localization of GFP-VSR2ΔCT was not observed by fluorescence microscopy (Figures 4 and 5), evidence for transit via the cell surface arose from the more sensitive drag-and-drop assay. Figure 9 shows that post-ER trafficking of flVSR2ΔCT results in cargo release at the cell surface, as measured by secretion of amy-spo to the culture medium. Introduction of the sequence QYMDSEIRA in the Δ23 deletion mutant increased the drag-and-drop activity of flVSR2Δ23 compared with the ΔCT construct (Figures 9B and 9C). This is consistent with the abolished ER retention of the corresponding fluorescent construct (GFP-VSR2Δ23). Further introduction of the IMAQ peptide in the Δ19 deletion mutant abolished the PM accumulation seen for Δ23 and instead resulted in PVC/LPVC partitioning. This could either be due to a decrease in exocytosis or increased endocytic recycling. The drag-and-drop assay specifically supports the latter option, because the flVSR2Δ19 construct mediated the strongest induced secretion of vacuolar cargo.

Together, these results suggest that bulk flow of a type I membrane-spanning protein such as the VSR leads from the ER to the Golgi, the TGN, and the PM but can proceed to the PVC, the LPVC, and the vacuole. This is in agreement with all previous reports (Barrieu and Chrispeels, 1999; Benghezal et al., 2000; Brandizzi et al., 2002; daSilva et al., 2006).

Biosynthetic VSR Targeting to the PVC Is Not by Bulk Flow and Avoids Transit via the PM

One of the key observations of this work is the evidence for at least two completely separate routes to the PVC in plants,

Figure 8. (continued).

(A) Confocal laser scanning micrographs of *Agrobacterium*-infiltrated tobacco leaf epidermis cells expressing GFP-VSR2 (the wild type), GFP-VSR2 (Y612A), GFP-VSR2(IMAA), or GFP-VSR2(IMAA+Y612A). Bars = 5 μm.

(B) Differential PVC/LPVC partitioning of GFP-VSR2Δ19 and GFP-VSR2Δ15 shown by confocal laser scanning micrographs of *Agrobacterium*-infiltrated tobacco leaf epidermis cells expressing either GFP-VSR2Δ19 or GFP-VSR2Δ15 with RFP-Rha1 expressed from the weak pNOS promoter. The cells are imaged at the cell cortex and shown in three-channel mode (green, red, and merged in yellow). White arrowheads indicate red-only LPVCs labeled with RFP-Rha1. Bars = 5 μm.

(C) Statistical correlation analysis of either GFP-VSR2Δ19 or GFP-VSR2Δ15 with the LPVC marker RFP-Rha1. The scatterplots are representative of at least 400 punctate structures, comprising a minimum of 50,000 pixels. The Spearman correlation coefficient (*r*) is shown for each deletion construct at the top right of the scatterplot. Bar charts show the results of the segmented population analysis, in which the sum of green and red signals is shown for each of the 16 bins. Note the sharp increase in red signals in bins 15 and 16 of Δ15 compared with Δ19, accompanied by a 2-fold reduction in the Spearman correlation coefficient.

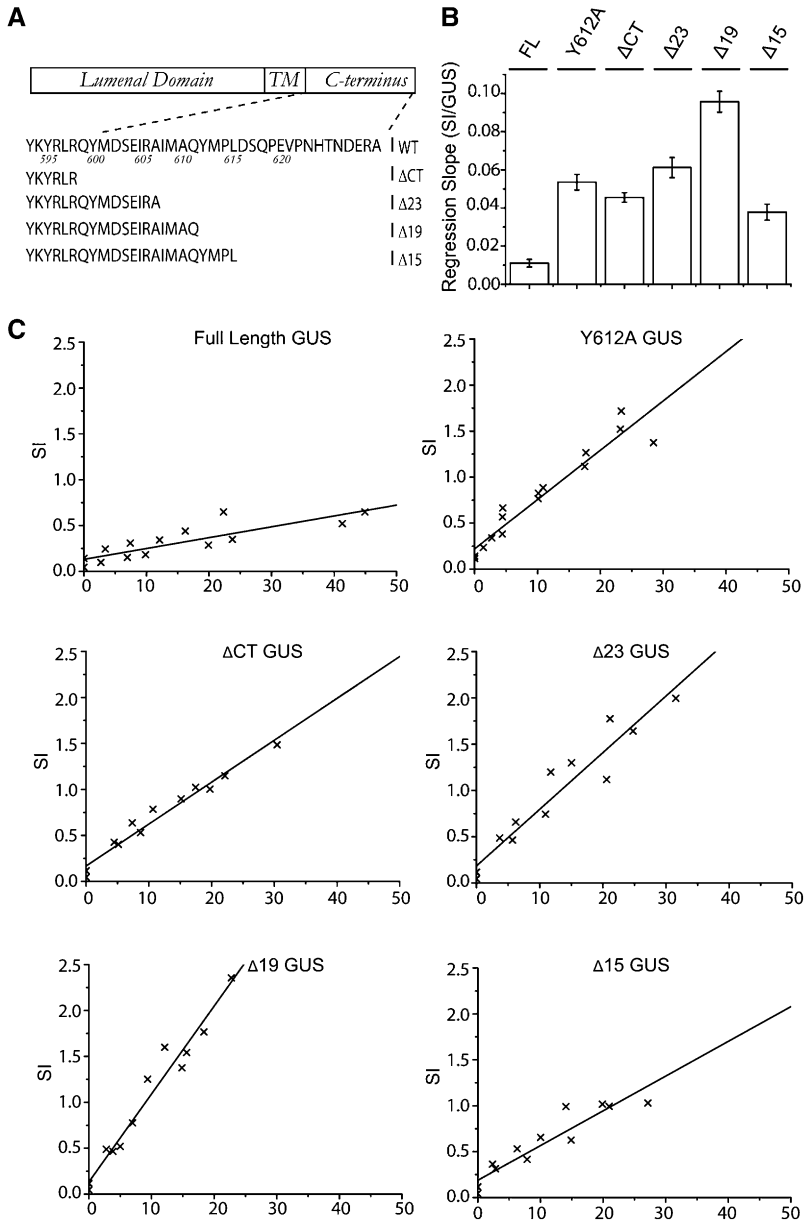

Figure 9. Biochemical Drag-and-Drop Assay to Monitor VSR Transit via the PM.

(A) Sequences of the individual deletion constructs used in this study. TM, transmembrane.

(B) Overview of the observed slopes from the individual dose–response assays for each construct, showing the inhibition of vacuolar sorting as a function of the internal GUS reference. Error bars represent SE of the distance of all data points from the individual calculated slopes in **(C)**.

(C) Individual X/Y scatter graphs illustrating individual secretion index (SI) data points (x) plotted as a function of internal GUS reference activity and linear regression lines.

a YMPL-mediated route that requires the conserved Glu-604 residue and a second YMPL-independent endocytic route. All constructs containing Y612A point mutations show strong cargo mistargeting to the PM (Figures 9 and 10). Complete deletion of the YMPL motif leads to even stronger missorting effects (compare Δ23 and Δ19 with all Y612A constructs). A functional YMPL motif within its natural peptide context is also dominant over the effect of long transmembrane domains in promoting PM partitioning (Figure 10).

The drag-and-drop assay reveals that one of the main functions of the YMPL motif is to prevent the arrival of receptors at the PM to avoid vacuolar cargo missorting (Figures 9 and 10). Therefore, VSR cycling via the PM is unlikely to have a biosynthetic function and merely represents endocytic rescue of mistargeted VSRs. IM-mediated VSR cycling via the PM may be

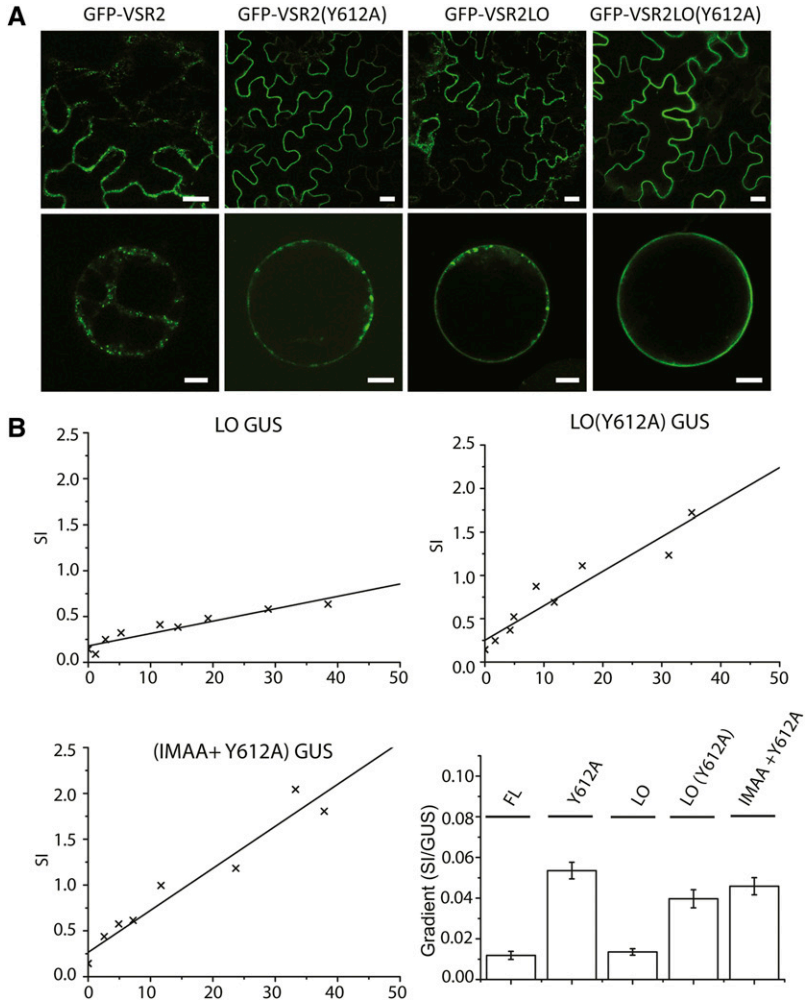

Figure 10. Influence of PM Partitioning on Drag-and-Drop Activity.

(A) Confocal laser scanning micrographs of *Agrobacterium*-infiltrated tobacco leaf epidermis cells expressing the four GFP-VSR2 fusions (top row) and protoplasts generated from stable transformed plants (bottom row). Individual constructs are indicated above each lane. Bars = 5 μm.
(B) Individual X/Y scatter graphs illustrating individual secretion index (SI) data points (x) plotted as a function of internal GUS reference activity and linear regression lines as well as an overview of observed gradients as a function of the internal GUS reference. Error bars represent SE of the distance of all data points from the calculated slope.

related to the recently described di-Leu signals for vacuolar membrane targeting in plants (Wolfenstetter et al., 2012; Xiang and Van den Ende, 2013). It could also play a role in specialized tissues where biosynthetic vacuolar sorting is not required while endocytic recycling is prevalent (i.e., growing pollen tubes) (Wang et al., 2010).

Selective VSR Trafficking to and from the PVC

Figure 11 illustrates a working model that can explain past and current data on receptor-mediated protein trafficking in the plant secretory pathway. Direct experimental evidence for Golgi-to-TGN trafficking remains to be obtained by the field; hence, two alternative routes are proposed for biosynthetic transport to the PVC (routes A1 and A2) and to the PM (routes B1 and B2). While ERD2 recycles to the ER upon ligand binding, causing rapid depletion of ER residents from *cis*- to *trans*-Golgi cisternae in plants (Phillipson et al., 2001), VSRs and their ligands would continue through the Golgi by cisternal progression, together with secretory bulk flow. Since VSRs carry hydrolases that should not be missorted to the cell surface, it is essential that they segregate from the secretory bulk flow by efficient selective retrieval. The direct TGN-to-PVC maturation model (Scheuring et al., 2011) cannot explain the different subcellular localizations of wild-type VSRs compared with the Y612A, L615A, ΔCT, Δ23, and Δ19 mutants, nor can it explain how vacuolar cargo segregates from the unselective bulk flow of soluble cargo to the cell surface (Denecke et al., 1990).

The critical role of the YMPL motif and the potential involvement of at least two distinct adaptor complexes in VSR trafficking (Figure 6) strongly support the principle that selective

carriers rather than organelle maturation mediate the Golgi/TGN-to-PVC transport of VSRs. This explains the copurification of VSRs with CCVs in three independent studies (Kirsch et al., 1994; Hinz et al., 1999; Sauer et al., 2013) and the involvement of two clathrin binding proteins (ENTH and ARF-GAP) in VSR cargo trafficking to the vacuole (Sauer et al., 2013). The potential involvement of AP4 in vacuolar sorting was unexpected, because in mammalian cells it has been proposed to act independently of clathrin (Dell'Angelica et al., 1999; Hirst et al., 1999). It remains to be established which type of coat is recruited by this adaptor complex, and a potential role of non-clathrin-coated carriers cannot be ignored. In mammalian cells, it has been proposed that AP4 could be a backup system when CCV-mediated transport becomes rate limiting (Hirst et al., 2012, 2013). This would explain why interference with clathrin-mediated transport has only weak effects on vacuolar sorting in plants (Scheuring et al., 2011; Sauer et al., 2013).

VSR recycling from the PVC is also signal mediated, requires the core fragment of retromer, and occurs from the PVC (Foresti et al., 2010; Saint-Jean et al., 2010; Kang et al., 2012). The selective recycling gives rise to the biochemically distinct LPVC, which is enriched in vacuolar cargo and at least a subset of rab5 GTPases (Foresti et al., 2010; Bottanelli et al., 2012). These punctate structures were observed with soluble fluorescent vacuolar cargo in transit to the vacuole in both *Arabidopsis* (Hunter et al., 2007; Jaillais et al., 2008) and tobacco (Foresti et al., 2010) and can now be used as noninvasive markers for the LPVC. Fluorescent rab5 fusions can only be used as LPVC markers when expressed at low levels to avoid interference with vacuolar sorting and associated merging of PVC and LPVC markers (Bottanelli et al., 2012). However, even with strong promoters in protoplasts, it was shown previously that fluorescent rab5 fusions and VSRs do not completely colocalize and that the noncolocalizing population of rab5 could not be the TGN (Lee et al., 2004). This is consistent with the existence of two types of multivesicular bodies, the PVC and the LPVC, as depicted in Figure 11.

Open Questions and Outlook

FM4-64 uptake studies (Dettmer et al., 2006; Lam et al., 2007a, 2007b) suggest that endocytic recycling from the PM first reaches

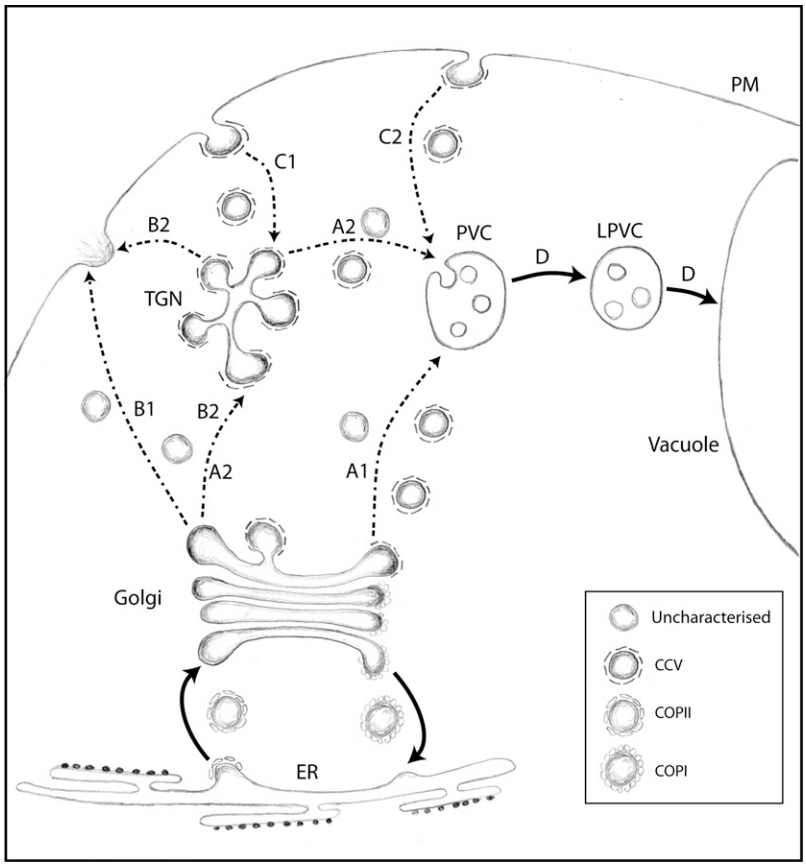

Figure 11. Working Model to Explain the Current Data Available on VSR Trafficking in Plants.

A simplified schematic of organelles and transport routes to the vacuole is shown. Organelles included are the ER, the Golgi apparatus, the partially coated reticulum or TGN, the PM, the PVC, the LPVC, and the vacuole. Known and unknown transport carriers are indicated in the boxed area. Dotted lines refer to pathways for which alternative routes cannot be excluded at present due to insufficient data. We consider two alternative or complementary biosynthetic routes to the PVC (A1 and A2). Likewise, two alternative routes must be considered for exocytosis at the PM (B1 and B2) and endocytosis from the PM (C1 and C2). The recycling route of the VSR is not shown.

the SYP61/41 compartment or TGN (Figure 11, route C1). However, the FM4-64 uptake route represents membrane bulk flow and may not be the only endocytic pathway in plants. It cannot be ruled out that mistargeted VSRs could be endocytosed via an active IM-mediated pathway leading directly to the PVC (route C2). Independent from the initial pathway, three different fates must be considered for endocytic cargo. It can recycle back to the PM, it may follow the lytic route to the PVC and beyond (route D), or it may recycle back to the Golgi apparatus, as reviewed (Bonifacino and Rojas, 2006). Likewise, if endocytosis of the Δ19 mutant leads to the TGN, part of it may continue to the PVC/LPVC system but another part may return to the PM (route B2) and mistarget further ligands to the cell surface. This could explain why the Δ19 mutant exhibits the strongest drag-and-drop effect (Figure 9). Future research will have to focus on using multiple endocytic markers and specifically investigate which transport steps are involved in trafficking to and from the TGN.

It is also still unknown where VSRs end up after they recycle from the PVC. It is plausible that VSRs return directly to the *trans*-Golgi cisternae, as it would explain why VSRs can be enriched in this compartment (Hillmer et al., 2001), but this remains to be shown. Tubular emanations from multivesicular bodies have been observed by electron microscopy and presented as evidence for TGN-to-PVC maturation (see Figures 4C and 4D in Scheuring et al., 2011). Due to the nature of fixed cell sections, however, the directionality of transport events cannot be interpreted from the reported still images, and they could equally represent the putative retromer carriers partitioned from the PVC membrane. Future research must determine the directionality (i.e., if these tubules are derived from or mature into multivesicular bodies). This will depend on fluorescent live-cell imaging to resolve donor membranes from their derived products as a function of time.

Finally, a potential role of AP4 in vacuolar sorting introduces an exciting member to the growing number of key elements in the plant secretory pathway that may help to resolve the complete transport cycle to the plant vacuole. It will be important to dissect the relative contributions of AP1- and AP4-mediated transport reactions. The rapid knock-sideways approach to deplete proteins and protein complexes at their site of action (Hirst et al., 2012) could be used to monitor protein mistargeting prior to cell mortality and perhaps to explore specific physiological conditions under which AP1 and AP4 play predominant roles. The subcellular localization of AP4 may help to establish if it plays an anterograde or retrograde trafficking role.

METHODS

Recombinant Plasmids

All DNA manipulations were performed according to standard procedures. *Escherichia coli* strain MC1061 (Casadaban and Cohen, 1980) was used for the preparation of competent *E. coli* stocks for the transformation of ligation mixtures of all plasmids. Previously established plasmids were used, encoding Amy and Amy-HDEL (Phillipson et al., 2001), amy-spo (Pimpl et al., 2003; daSilva et al., 2005), Aleu-Amy, Aleu-RFP (Bottanelli et al., 2011), GFP-VSR2 (previously called GFP-BP80), GFP-VSR2(Y612A), GFP-VSR2(L615A), GFP-VSR2ΔCT, full-length VSR2, and full-length VSR2(Y612A) (daSilva et al., 2005, 2006). All oligonucleotide sequences for new plasmids built and used in this study are named and listed in Supplemental Table 1.

To generate the dual-signal cargo Aleu-RFP-HDEL, the above-listed Aleu-RFP plasmid was used as a template for PCR amplification using primers 35Ssense and RFP-HDEL-anti. The resulting fragment was digested with *Cla*I and *Bam*HI, which extracts a hybrid coding region carrying a signal peptide and N-terminal region of barley (*Hordeum vulgare*) aleurain fused to the N terminus of the RFP coding region, followed by the HDEL-encoding sequence (Aleu-RFP-HDEL), and used to replace the RFP-VSR2 coding region in the plant vector described previously (Foresti et al., 2010). RFP-HDEL was generated using the same primer pair as Aleu-RFP-HDEL, except that RFP-VSR2 was used as a template to obtain a hybrid coding region comprising a signal peptide fused to the N terminus of RFP. Sec-RFP was extracted from RFP-VSR2 by cutting with *Cla*I and *Bgl*II to obtain a hybrid coding region comprising a signal peptide fused to the N terminus of RFP without the VSR C terminus and ligated together with a *Bgl*II-*Hin*dIII 3′nos fragment extracted from pTAmy (Phillipson et al., 2001) to replace RFP-VSR2 in the plant vector described previously (Foresti et al., 2010). This regenerates the stop codon at the end of the RFP coding region.

To create a low-expressed construct for the LPVC marker Rha1 (Foresti et al., 2010; Bottanelli et al., 2012), the weak nopaline synthase promoter was amplified from the *Agrobacterium tumefaciens* transformation vector pDE1001 (Denecke et al., 1992) using the primer pair pNOS-sense and pNOS-anti, cut with *Eco*RI and *Cla*I, and gel purified. For in-frame fusion with the Rha1 coding region, the RFP coding region was amplified with the primer pair RFPClaI-sense and RFPNcoI-anti, cut with *Cla*I and *Nco*I, and gel purified. A DNA fragment with the Rha1 coding region followed by the 3′ untranslated end of nopaline synthase carrying the polyadenylation signal (3′nos) was cut from the plasmid pTDCG9 (Foresti et al., 2010) with *Nco*I and *Hin*dIII and gel purified. The three fragments were ligated into the polylinker of pGSC1700 (Cornelissen and Vandewiele, 1989), cut with *Eco*RI and *Hin*dIII, and dephosphorylated, to yield the pNOS-RFP-Rha1 plant expression construct (pTCM72).

The GUS reference vector (Supplemental Figure 1) for normalized dose–response analysis via transient expression of different effector molecules was built using a simultaneous enzymatic isothermal multiple-fragment assembly as described (Gibson et al., 2009), here termed a Gibson assembly, in order to build a plasmid that includes a hybrid gene containing the TR2′ promoter fused to the GUS coding region followed by the 3′ untranslated end of octopine synthase carrying the polyadenylation signal (3′ocs) and avoiding the use of popular restriction sites, thus maximizing the number of unique cloning sites available for insertion of the test gene for effector analysis (Supplemental Figure 1). Four PCR fragments representing the TR2′ promoter, the GUS coding region, the 3′ocs polyadenylation signal followed by a polylinker, and the 3′nos polyadenylation signal, as well as a linearized pUC19 vector (*Eco*RI-*Hin*dIII), were used to assemble a newly designed plasmid with a large polylinker of unique sites (Supplemental Figure 1).

To generate deletions in the cytosolic tail of VSR2, the primers delta23-anti, delta19-anti, and delta15-anti were used as antisense primers (Supplemental Table 1). For all GFP-VSR2 fusions, these antisense primers were used in conjunction with 35S-sense, and amplified fragments were cloned as *Nco*I-*Xba*I fragments to replace the second half of GFP and the fused VSR2 wild-type sequence by the appropriate deletions. In the case of full-length VSR2, the corresponding plant expression plasmid described (daSilva et al., 2006) was used as a template and amplified with pUCsense and each of the three deletion antisense primers to obtain three amplified fragments, which were digested with *Eco*RI and *Xba*I to extract fragments comprising the 35S promoter and full-length VSR2 minus the appropriate deleted portions, to be subcloned into the GUS reference vector described above.

GFP-VSR2ΔCT-NFLET was generated by amplifying from the GFP-VSR2wt template using the primers 35S-sense and NFLET to yield a product subsequently digested using *Nco*I and *Xba*I and subcloned into the GFP-VSR2wt vector prepared using the same enzymes, as described above for GFP-VSR2Δ23/19/15.

For the yeast two-hybrid analysis, the VSR2wt C terminus was used as bait. The region encoding the VSR2 terminus was amplified using the primers BP80tailY2H and pUCOF from VSR2wt and subcloned into the multiple cloning site in pGBKT7 (Clontech Laboratories) using the enzymes *Nco*I and *Bam*HI. The plant μ-adaptins were amplified from an *Arabidopsis thaliana* cDNA library using the AP1-4sense and antisense primers and subsequently subcloned into the multiple cloning site of the prey vector pGADT7 (Clontech Laboratories) as blunt-*Bam*HI fragments.

The constructs encoding mammalian μ-subunits, mu1A (mouse), mu1B (human), mu2 (mouse), mu3A (rat), and mu4 (human), in pACT2 have been described previously (Ohno et al., 1999; Guo et al., 2013). The construct encoding the cytosolic tail of TGN38 in pGBT9 was described previously (Ohno et al., 1996). Mammalian μ-adaptin and TGN38 constructs were generously provided by Juan S. Bonifacino.

All point mutations described in this article were performed using the QuickChange method (Stratagene) on small pUC-based plasmids carrying the recombinant coding regions, followed by sequencing, using the primer pairs and templates described (Supplemental Table 1). Further point mutations included a primer pair to generate the DSE-to-ASA double mutant (ASA-sense and ASA-anti), a pair to generate the IMAA double mutant (IMAA-sense and IMAA-anti), and a pair to impose the Y612A mutation onto the IMAA mutant (IMAAY-sense and IMAAY-anti). Sequence-verified chimeric genes were then routinely inserted as *Eco*RI-*Hin*dIII fragments into the polylinker of the *Agrobacterium* transformation vector pDE1001 (Denecke et al., 1992) for leaf infiltration experiments or into the GUS reference vector described above for quantitative dose–response assays.

To produce VSR2 derivatives with a long transmembrane domain, the QuickChange method (Stratagene) was used with pairs of oligonucleotides (LO-sense and LO-anti) comprising the inserted 12 nucleotides encoding the peptide Ala-Leu-Ala-Leu and 21 bases extending on either side of the inserted sequence (Supplemental Table 1). This strategy was applied to plasmids encoding GFP-VSR2, GFP-VSR2(Y612A), full-length VSR2, or full-length VSR2(Y612A), followed by sequencing and subcloning into the plant vector for *Agrobacterium*-mediated transformation (pDE1001 and derivatives) or the GUS reference vector described above.

All plant transformation plasmids were transfected into the *Agrobacterium* rifampicin-resistant strain C58C1RifR (pGV2260) to generate the binary plant transformation strains, streaked twice on selective medium as described previously (Denecke et al., 1992), and kept as 15% glycerol stocks at −80°C.

Yeast Two-Hybrid Assays

Saccharomyces cerevisiae strain AH-109 (Clontech) was maintained on YPD agar plates. Transformation was performed by the lithium acetate procedure with combinations of plasmids encoding the different μ-adaptins and the cytosolic tail of VSR2 or TGN38, as described in the instructions of the Matchmaker two-hybrid kit (Clontech). Mouse p53 fused to Gal4BD and SV40 large T antigen fused to Gal4AD were used as controls. Cotransformants were selected by growth on plates lacking Leu and Trp containing His (+HIS). For interaction assay, AH-109 cotransformants were spotted on plates lacking Leu and Trp (+HIS) or lacking Leu, Trp, and His (−HIS) and allowed to grow at 30°C for 3 to 5 d. Growth on plates lacking His is indicative of interactions.

Plant Material and Standard Transient Protoplast Expression Procedure

Sterile-grown tobacco (*Nicotiana tabacum* cv Petit Havana) (Maliga et al., 1973) plants were grown from surface-sterilized seeds. Typically, 20 mg of tobacco seeds was incubated for 30 min in 1 mL of 10% bleach supplemented with 0.1% Tween 20 in a microfuge tube, washed 5-fold with 1 mL of autoclaved distilled water, followed by placing on the surface of Murashige and Skoog medium (Murashige and Skoog, 1962) supplemented with 2% Suc and incubation in a controlled room at 22°C with a 16-h daylength at a light irradiance of 200 mE m^{-2} s^{-1}. After 2 weeks of incubation, individual seedlings were lifted out and planted individually in glass jars for an additional 3- to 6-week incubation under the same conditions to create sufficient sterile leaves for transient expression analysis. Preparation of tobacco leaf protoplasts and standard transient expression analysis via electroporation, protoplast incubation, harvesting cells and medium, as well as measurement of α-amylase activity and calculation of the secretion index (ratio of extracellular to intracellular enzyme activities) were done as described previously (Foresti et al., 2006).

Combined α-Amylase Activity and Protein Extraction and Gel Blot Analysis

To monitor the effect of COPII transport inhibitors on constitutive secretion in conjunction with the proteolytic processing of GFP-VSR2, the following working practice was followed. A standard transient expression was performed (Foresti et al., 2006), and after sampling of the undiluted protoplast culture medium, protoplast pellets obtained from the 2.5-mL suspensions after being washed in 10 mL of 250 mM NaCl were drained using a Pasteur pipette connected to a peristaltic pump and resuspended using 200 μL of ice-cold α-amylase extraction buffer. By weighing the microfuge tubes before and after addition of the resuspended cells in α-amylase extraction buffer, tubes were supplemented with the required amount of α-amylase extraction buffer to bring each extract to exactly 250 μL of extraction mix (pellet + extraction buffer) to be sonicated, centrifuged at 15,000 rpm and 4°C for 10 min, and analyzed together with the medium sample as described before to calculate the amylase secretion index (Foresti et al., 2006).

The supernatant of the sonicated centrifuged cells contains cellular α-amylase as well as the soluble vacuolar degradation product of the GFP-VSR2 fusion. Fifty microliters of this supernatant was diluted with 50 μL of SDS-PAGE sample buffer and kept for protein gel blots (soluble protein sample). The pellet contains membrane proteins and was extracted by sonication with 250 μL of ice-cold membrane protein extraction buffer (100 mM Tris-HCl, pH 7.8, 200 mM NaCl, 1 mM EDTA, 0.2% Triton X-100, and 2% β-mercaptoethanol), followed by centrifugation at 15,000 rpm (25,000*g*) and 4°C for 10 min. Fifty microliters of the obtained supernatant was diluted with 50 μL of SDS-PAGE sample buffer (membrane protein sample) and analyzed together with the soluble protein sample described above by protein gel blot analysis as described previously (Pimpl et al., 2006). For immunodetection, we used rabbit polyclonal antiserum raised against GFP (1:5000 dilution; Molecular Probes).

GUS-Normalized Effector Dose–Response Assays

The quantification of GUS activity from the internal reference gene on the GUS reference plasmid allows for accurate dose–response analysis for the comparison of different effector molecules that takes full account of transfection efficiency. All effector constructs built into the GUS reference plasmid were first tested for GUS expression alone. Poorly transfecting plasmid preparations were discarded and replaced by new preparations that yielded acceptable GUS expression. A typical dose–response assay would then constitute of a series of transfections in which a constant amount of vacuolar cargo (amy-spo)–encoding plasmid coelectroporated with a dilution series of the appropriate GUS effector plasmids. The resulting samples were then tested again for GUS activity as well as α-amylase activity in medium and cells for calculation of the secretion index.

The following working practice was employed. From the 2.5-mL protoplast suspension from a standard electroporation after 24 h of incubation at 22°C, suspensions were gently swirled to allow mixing of protoplasts and medium, after which 500 μL was transferred to a 1.5-mL microcentrifuge tube containing 500 μL of GUS extraction buffer and kept on ice (50 mM sodium phosphate buffer, pH 7.0, 10 mM Na_2EDTA, 0.1% sodium lauryl sarcosine, 0.1% Triton X-100, and 10 mM β-mercaptoethanol). The mixed GUS extraction samples on ice (1 mL) were first

sonicated (40% for 10 s), vortexed, and centrifuged at 15,000 rpm and 4°C for 10 min. One hundred microliters of each supernatant was then divided into aliquots on a 96-well microtiter plate and mixed with 100 μL of the GUS reaction buffer (50 mM sodium phosphate buffer, pH 7.0, 0.1% Triton X-100, 2 mM 4-nitrophenyl-β-D-glucopyranosiduronic acid, and 10 mM β-mercaptoethanol). These samples were then incubated at 37°C, typically for 2 h, before being stopped with 80 μL of 2.5 M 2-amino-2-methyl propanediol. As a negative control, an extract from a mock-electroporated sample was analyzed in the same way to distinguish the background of pigments from the yellow *para*-nitrophenol released by the enzyme. A second complementary control was a zero stop for all samples: 80 μL of GUS stop buffer was added before the addition of GUS reaction buffer, mixed, and incubated for 2 h. The optical absorbance of all test and zero reactions was then directly measured on the microtiter plate at λ405. The ODs measured for the individual zero stops were then subtracted from the ODs measured from the corresponding sample test readings. Due to the nonlinearity of the reaction, a standard curve was constructed and all samples were normalized to the factor $y = -0.0003x^2 + 0.0643x + 0.0085$ [where y = sample OD(λ405)], to obtain the corrected GUS activity values.

During the period in which the GUS assays were incubating, cells and medium of the remaining 2-mL cell suspension were harvested into cell and medium samples for subsequent α-amylase activity measurement as described before (Foresti et al., 2006), except that all volumetric calculations were based on a 2-mL total suspension rather than the standard 2.5 mL. Finally, the calculated secretion indices were then plotted as a function of the corresponding corrected GUS activities for each sample to obtain an X/Y scatterplot, followed by linear regression of the corresponding slope (gradient) to establish a dose response. Figures in this article show individual X/Y scatterplots supplemented with linear regression lines to visualize the experimental data. Furthermore, individual gradients are shown in bar charts for direct comparison of different effectors, including the deviation from the line as error bars.

Tobacco Leaf Infiltration Procedure

Soil-grown tobacco plants were infiltrated with overnight cultures of *Agrobacterium* grown in mannitol glutamate luria medium, diluted to an OD of 0.1 at 600 nm, and infiltrated into leaves of 5-week-old soil-grown tobacco cultivar Petit Havana (Maliga et al., 1973), as described previously (Sparkes et al., 2006). Confocal laser scanning microscopy analysis was done 48 h after infiltration, unless otherwise indicated in the figure legends.

Fluorescence Confocal Microscopy Imaging and Analysis

Infiltrated tobacco leaf squares (0.5 × 0.5 cm) were mounted in tap water with the lower epidermis facing the thin cover glass (22 × 50 mm; No. 0). Protoplasts from transgenic plants were mounted on slides supplemented with 0.1 mm of electrical tape with a cut-out square of 1 × 1 cm to create a well for the protoplast suspension between the slide and the cover glass, as described previously (daSilva et al., 2005, 2006). Confocal imaging was performed using an inverted Zeiss LSM 700 laser scanning microscope. When GFP fusions were imaged with RFP organelle markers, samples were excited with a diode laser at the wavelength of 488 nm for GFP and 555 nm for RFP. Fluorescence was detected with a 552-nm dichroic beam splitter and a 475- to 550-nm bandpass filter for GFP and a 560- to 700-nm bandpass filter for RFP. All dual-color imaging was performed by line switching to obtain adequate live bioimaging data that are not distorted by organelle motion. For single-color imaging, an upright Zeiss LSM 510 META laser scanning microscope with a Plan-Neofluar ×40/1.3 oil differential interference contrast objective was used, employing the excitation lines of an argon ion laser of 488 nm and a 500- to 530-nm narrow bandpass filter for detection of GFP. For imaging of the coexpression of GFP and RFP constructs, or Venus and RFP constructs, excitation lines of an argon ion laser of 488 nm for GFP/Venus and of a helium/neon laser of 543 nm for RFP were used alternately with line switching on the multitrack facility of the microscope. Fluorescence was detected using a 545-nm dichroic beam splitter for GFP/Venus and a 565- to 615-nm bandpass filter for RFP. Postacquisition image processing was performed with the LSM 5 image browser (Zeiss), the Zen 2011 blue edition (Zeiss), and ImageJ (http://rsbweb.nih.gov/ij/download.html).

Image analysis was undertaken using the ImageJ analysis program and the PSC colocalization plugin (French et al., 2008) to calculate colocalization and to produce scatterplots. The degree of correlation is given as the Spearman rank correlation coefficient, and the PSC colocalization plugin generates values in the range [−1, +1], where +1 indicates the strongest positive correlation, 0 indicates no correlation, and −1 indicates the strongest negative correlation. The shape of the scatterplots indicates more complex scenarios, including a combination of correlating and noncorrelating pixel populations, as well as specific shifts in red:green ratios (Bottanelli et al., 2011, 2012). At least 20 images comprising a minimum of 400 independent punctate structures were analyzed for each condition, and punctate structures were selected using the selection brush tool as described (French et al., 2008; Foresti et al., 2010). A threshold level of 10 was set, under which pixel values were considered noise and not included in the statistical analysis.

Segmented population analysis of scatterplots was performed to document specific population shifts in a partial colocalization experiment, as introduced previously (Bottanelli et al., 2012). Scatterplots were subdivided into 16 pie segments of equal surface, representing data bins of 16 different categories with progressively increasing red:green ratios (from left to right). The first bin comprises all pixels that have a red:green ratio between 0 and 6.25% red, the second bin includes ratios from 6.25 to 12.5% red, and so on until the 16th and final bin, which includes 93.75 to 100% red. The obtained bar charts show the amount of green and red signals in each bin, progressing from predominantly green (left) to red (right).

Accession Numbers

Sequence data from this article can be found in the GenBank/EMBL libraries under the following accession numbers: muAP1A (AT1G60780), muAP1B (AT1G10730), muAP2 (AT5G46630), muAP3 (AT1G56590), and muAP4 (AT4G24550).

Supplemental Data

The following materials are available in the online version of this article.

Supplemental Figure 1. Restriction Map of pGUS Reference.

Supplemental Table 1. Primers Used in This Study.

ACKNOWLEDGMENTS

We thank Juan Bonifacino (National Institutes of Health) for sharing the mammalian μ-adaptin and TGN38 constructs with us. Veritas (in Leeds) is thanked for all the good hours discussing science and jazz. We also thank Gareth Howell (University of Leeds) for scientific discussion, ad hoc troubleshooting with the BioImaging Facility at Leeds, and prompt correspondence at impossible working hours. The work in this article was supported by the European Union (Grants HPRN-CT-2002-00262 and LSH-2002-1.2.5-2), the Biotechnology and Biological Sciences Research Council (responsive mode grant BB/D016223/1 and a doctoral training grant to D.C.G.), the Leverhulme Trust (Grant F/10 105/E)., the University of Leeds (international research scholarship to F.B.), the Brazilian National Council for Scientific and Technological Development (research scholarship to E.A.P.), the Coordenação de Aperfeiçoamento de Pessoal de Nível Superior, Brazilian Ministry of Education (PhD studentship to L.L.P.d.), and

the Fundaçào de Amparo à Pesquisa do Estado de São Paulo (Young Investigator's Award 2009/50650-6 to L.L.P.d.).

AUTHOR CONTRIBUTIONS

D.C.G. and J.D. conceived and designed the research. D.C.G., C.d.M.L., O.F., A.J.L., E.A.P., L.L.P.d., F.B., and J.D. performed research and analyzed data. D.C.G. contributed new analytic and computational tools. D.C.G., C.d.M.L., and J.D. wrote the article.

Received December 20, 2013; revised February 10, 2014; accepted February 18, 2014; published March 18, 2014.

REFERENCES

Barlowe, C., Orci, L., Yeung, T., Hosobuchi, M., Hamamoto, S., Salama, N., Rexach, M.F., Ravazzola, M., Amherdt, M., and Schekman, R. (1994). COPII: A membrane coat formed by Sec proteins that drive vesicle budding from the endoplasmic reticulum. Cell **77:** 895–907.

Barrieu, F., and Chrispeels, M.J. (1999). Delivery of a secreted soluble protein to the vacuole via a membrane anchor. Plant Physiol. **120:** 961–968.

Benghezal, M., Wasteneys, G.O., and Jones, D.A. (2000). The C-terminal dilysine motif confers endoplasmic reticulum localization to type I membrane proteins in plants. Plant Cell **12:** 1179–1201.

Bonifacino, J.S., and Rojas, R. (2006). Retrograde transport from endosomes to the trans-Golgi network. Nat. Rev. Mol. Cell Biol. **7:** 568–579.

Bottanelli, F., Foresti, O., Hanton, S., and Denecke, J. (2011). Vacuolar transport in tobacco leaf epidermis cells involves a single route for soluble cargo and multiple routes for membrane cargo. Plant Cell **23:** 3007–3025.

Bottanelli, F., Gershlick, D.C., and Denecke, J. (2012). Evidence for sequential action of Rab5 and Rab7 GTPases in prevacuolar organelle partitioning. Traffic **13:** 338–354.

Brandizzi, F., and Barlowe, C. (2013). Organization of the ER-Golgi interface for membrane traffic control. Nat. Rev. Mol. Cell Biol. **14:** 382–392.

Brandizzi, F., Frangne, N., Marc-Martin, S., Hawes, C., Neuhaus, J.M., and Paris, N. (2002). The destination for single-pass membrane proteins is influenced markedly by the length of the hydrophobic domain. Plant Cell **14:** 1077–1092.

Casadaban, M.J., and Cohen, S.N. (1980). Analysis of gene control signals by DNA fusion and cloning in *Escherichia coli*. J. Mol. Biol. **138:** 179–207.

Cereghino, J.L., Marcusson, E.G., and Emr, S.D. (1995). The cytoplasmic tail domain of the vacuolar protein sorting receptor Vps10p and a subset of VPS gene products regulate receptor stability, function, and localization. Mol. Biol. Cell **6:** 1089–1102.

Ceriotti, A., and Colman, A. (1988). Binding to membrane proteins within the endoplasmic reticulum cannot explain the retention of the glucose-regulated protein GRP78 in Xenopus oocytes. EMBO J. **7:** 633–638.

Chatre, L., Wattelet-Boyer, V., Melser, S., Maneta-Peyret, L., Brandizzi, F., and Moreau, P. (2009). A novel di-acidic motif facilitates ER export of the syntaxin SYP31. J. Exp. Bot. **60:** 3157–3165.

Cooper, A.A., and Stevens, T.H. (1996). Vps10p cycles between the late-Golgi and prevacuolar compartments in its function as the sorting receptor for multiple yeast vacuolar hydrolases. J. Cell Biol. **133:** 529–541.

Cornelissen, M., and Vandewiele, M. (1989). Nuclear transcriptional activity of the tobacco plastid psbA promoter. Nucleic Acids Res. **17:** 19–29.

Crofts, A.J., Leborgne-Castel, N., Hillmer, S., Robinson, D.G., Phillipson, B., Carlsson, L.E., Ashford, D.A., and Denecke, J. (1999). Saturation of the endoplasmic reticulum retention machinery reveals anterograde bulk flow. Plant Cell **11:** 2233–2248.

daSilva, L.L., Foresti, O., and Denecke, J. (2006). Targeting of the plant vacuolar sorting receptor BP80 is dependent on multiple sorting signals in the cytosolic tail. Plant Cell **18:** 1477–1497.

daSilva, L.L., Snapp, E.L., Denecke, J., Lippincott-Schwartz, J., Hawes, C., and Brandizzi, F. (2004). Endoplasmic reticulum export sites and Golgi bodies behave as single mobile secretory units in plant cells. Plant Cell **16:** 1753–1771.

daSilva, L.L., Taylor, J.P., Hadlington, J.L., Hanton, S.L., Snowden, C.J., Fox, S.J., Foresti, O., Brandizzi, F., and Denecke, J. (2005). Receptor salvage from the prevacuolar compartment is essential for efficient vacuolar protein targeting. Plant Cell **17:** 132–148.

Dell'Angelica, E.C., Mullins, C., and Bonifacino, J.S. (1999). AP-4, a novel protein complex related to clathrin adaptors. J. Biol. Chem. **274:** 7278–7285.

De Marcos Lousa, C., Gershlick, D.C., and Denecke, J. (2012). Mechanisms and concepts paving the way towards a complete transport cycle of plant vacuolar sorting receptors. Plant Cell **24:** 1714–1732.

Denecke, J., Botterman, J., and Deblaere, R. (1990). Protein secretion in plant cells can occur via a default pathway. Plant Cell **2:** 51–59.

Denecke, J., De Rycke, R., and Botterman, J. (1992). Plant and mammalian sorting signals for protein retention in the endoplasmic reticulum contain a conserved epitope. EMBO J. **11:** 2345–2355.

Dettmer, J., Hong-Hermesdorf, A., Stierhof, Y.D., and Schumacher, K. (2006). Vacuolar H^+-ATPase activity is required for endocytic and secretory trafficking in *Arabidopsis*. Plant Cell **18:** 715–730.

Dorel, C., Voelker, T.A., Herman, E.M., and Chrispeels, M.J. (1989). Transport of proteins to the plant vacuole is not by bulk flow through the secretory system, and requires positive sorting information. J. Cell Biol. **108:** 327–337.

Foresti, O., daSilva, L.L., and Denecke, J. (2006). Overexpression of the *Arabidopsis* syntaxin PEP12/SYP21 inhibits transport from the prevacuolar compartment to the lytic vacuole in vivo. Plant Cell **18:** 2275–2293.

Foresti, O., Gershlick, D.C., Bottanelli, F., Hummel, E., Hawes, C., and Denecke, J. (2010). A recycling-defective vacuolar sorting receptor reveals an intermediate compartment situated between prevacuoles and vacuoles in tobacco. Plant Cell **22:** 3992–4008.

French, A.P., Mills, S., Swarup, R., Bennett, M.J., and Pridmore, T.P. (2008). Colocalization of fluorescent markers in confocal microscope images of plant cells. Nat. Protoc. **3:** 619–628.

Gibson, D.G., Young, L., Chuang, R.Y., Venter, J.C., Hutchison, C.A., III., and Smith, H.O. (2009). Enzymatic assembly of DNA molecules up to several hundred kilobases. Nat. Methods **6:** 343–345.

Guo, X., Mattera, R., Ren, X., Chen, Y., Retamal, C., González, A., and Bonifacino, J.S. (2013). The adaptor protein-1 μ1B subunit expands the repertoire of basolateral sorting signal recognition in epithelial cells. Dev. Cell **27:** 353–366.

Hanton, S.L., Renna, L., Bortolotti, L.E., Chatre, L., Stefano, G., and Brandizzi, F. (2005). Diacidic motifs influence the export of transmembrane proteins from the endoplasmic reticulum in plant cells. Plant Cell **17:** 3081–3093.

Happel, N., Höning, S., Neuhaus, J.M., Paris, N., Robinson, D.G., and Holstein, S.E. (2004). Arabidopsis mu A-adaptin interacts with the tyrosine motif of the vacuolar sorting receptor VSR-PS1. Plant J. **37:** 678–693.

Hara-Nishimura, I., Shimada, T., Hatano, K., Takeuchi, Y., and Nishimura, M. (1998). Transport of storage proteins to protein

storage vacuoles is mediated by large precursor-accumulating vesicles. Plant Cell **10:** 825–836.

Herman, E.M., and Larkins, B.A. (1999). Protein storage bodies and vacuoles. Plant Cell **11:** 601–614.

Hillmer, S., Movafeghi, A., Robinson, D.G., and Hinz, G. (2001). Vacuolar storage proteins are sorted in the cis-cisternae of the pea cotyledon Golgi apparatus. J. Cell Biol. **152:** 41–50.

Hinz, G., Hillmer, S., Baumer, M., and Hohl, I.I. (1999). Vacuolar storage proteins and the putative vacuolar sorting receptor BP-80 exit the Golgi apparatus of developing pea cotyledons in different transport vesicles. Plant Cell **11:** 1509–1524.

Hirst, J., Borner, G.H., Antrobus, R., Peden, A.A., Hodson, N.A., Sahlender, D.A., and Robinson, M.S. (2012). Distinct and overlapping roles for AP-1 and GGAs revealed by the "knocksideways" system. Curr. Biol. **22:** 1711–1716.

Hirst, J., Bright, N.A., Rous, B., and Robinson, M.S. (1999). Characterization of a fourth adaptor-related protein complex. Mol. Biol. Cell **10:** 2787–2802.

Hirst, J., Irving, C., and Borner, G.H. (2013). Adaptor protein complexes AP-4 and AP-5: New players in endosomal trafficking and progressive spastic paraplegia. Traffic **14:** 153–164.

Hunter, P.R., Craddock, C.P., Di Benedetto, S., Roberts, L.M., and Frigerio, L. (2007). Fluorescent reporter proteins for the tonoplast and the vacuolar lumen identify a single vacuolar compartment in Arabidopsis cells. Plant Physiol. **145:** 1371–1382.

Jaillais, Y., Fobis-Loisy, I., Miège, C., and Gaude, T. (2008). Evidence for a sorting endosome in Arabidopsis root cells. Plant J. **53:** 237–247.

Kang, H., Kim, S.Y., Song, K., Sohn, E.J., Lee, Y., Lee, D.W., Hara-Nishimura, I., and Hwang, I. (2012). Trafficking of vacuolar proteins: The crucial role of *Arabidopsis* vacuolar protein sorting 29 in recycling vacuolar sorting receptor. Plant Cell **24:** 5058–5073.

Kim, H., Kang, H., Jang, M., Chang, J.H., Miao, Y.S., Jiang, L.W., and Hwang, I. (2010). Homomeric interaction of AtVSR1 is essential for its function as a vacuolar sorting receptor. Plant Physiol. **154:** 134–148.

Kirchhausen, T., Bonifacino, J.S., and Riezman, H. (1997). Linking cargo to vesicle formation: Receptor tail interactions with coat proteins. Curr. Opin. Cell Biol. **9:** 488–495.

Kirsch, T., Paris, N., Butler, J.M., Beevers, L., and Rogers, J.C. (1994). Purification and initial characterization of a potential plant vacuolar targeting receptor. Proc. Natl. Acad. Sci. USA **91:** 3403–3407.

Kleine-Vehn, J., Leitner, J., Zwiewka, M., Sauer, M., Abas, L., Luschnig, C., and Friml, J. (2008). Differential degradation of PIN2 auxin efflux carrier by retromer-dependent vacuolar targeting. Proc. Natl. Acad. Sci. USA **105:** 17812–17817.

Kural, C., Tacheva-Grigorova, S.K., Boulant, S., Cocucci, E., Baust, T., Duarte, D., and Kirchhausen, T. (2012). Dynamics of intracellular clathrin/AP1- and clathrin/AP3-containing carriers. Cell Rep. **2:** 1111–1119.

Lam, S.K., Siu, C.L., Hillmer, S., Jang, S., An, G., Robinson, D.G., and Jiang, L. (2007a). Rice SCAMP1 defines clathrin-coated, trans-Golgi–located tubular-vesicular structures as an early endosome in tobacco BY-2 cells. Plant Cell **19:** 296–319.

Lam, S.K., Tse, Y.C., Robinson, D.G., and Jiang, L. (2007b). Tracking down the elusive early endosome. Trends Plant Sci. **12:** 497–505.

Lee, G.J., Sohn, E.J., Lee, M.H., and Hwang, I. (2004). The Arabidopsis rab5 homologs rha1 and ara7 localize to the prevacuolar compartment. Plant Cell Physiol. **45:** 1211–1220.

Maliga, P., Sz-Breznovits, A., and Márton, L. (1973). Streptomycin-resistant plants from callus culture of haploid tobacco. Nat. New Biol. **244:** 29–30.

Mercanti, V., Marchetti, A., Lelong, E., Perez, F., Orci, L., and Cosson, P. (2010). Transmembrane domains control exclusion of membrane proteins from clathrin-coated pits. J. Cell Sci. **123:** 3329–3335.

Murashige, T., and Skoog, F. (1962). A revised medium for rapid growth and bio assays with tobacco tissue cultures. Physiol. Plant. **15:** 473–497.

Niemes, S., Labs, M., Scheuring, D., Krueger, F., Langhans, M., Jesenofsky, B., Robinson, D.G., and Pimpl, P. (2010a). Sorting of plant vacuolar proteins is initiated in the ER. Plant J. **62:** 601–614.

Niemes, S., Langhans, M., Viotti, C., Scheuring, D., San Wan Yan, M., Jiang, L., Hillmer, S., Robinson, D.G., and Pimpl, P. (2010b). Retromer recycles vacuolar sorting receptors from the trans-Golgi network. Plant J. **61:** 107–121.

Nishimura, N., and Balch, W.E. (1997). A di-acidic signal required for selective export from the endoplasmic reticulum. Science **277:** 556–558.

Nishimura, N., Bannykh, S., Slabough, S., Matteson, J., Altschuler, Y., Hahn, K., and Balch, W.E. (1999). A di-acidic (DXE) code directs concentration of cargo during export from the endoplasmic reticulum. J. Biol. Chem. **274:** 15937–15946.

Ohno, H., Fournier, M.C., Poy, G., and Bonifacino, J.S. (1996). Structural determinants of interaction of tyrosine-based sorting signals with the adaptor medium chains. J. Biol. Chem. **271:** 29009–29015.

Ohno, H., Tomemori, T., Nakatsu, F., Okazaki, Y., Aguilar, R.C., Foelsch, H., Mellman, I., Saito, T., Shirasawa, T., and Bonifacino, J.S. (1999). Mu1B, a novel adaptor medium chain expressed in polarized epithelial cells. FEBS Lett. **449:** 215–220.

Park, M., Song, K., Reichardt, I., Kim, H., Mayer, U., Stierhof, Y.D., Hwang, I., and Jürgens, G. (2013). Arabidopsis μ-adaptin subunit AP1M of adaptor protein complex 1 mediates late secretory and vacuolar traffic and is required for growth. Proc. Natl. Acad. Sci. USA **110:** 10318–10323.

Pelham, H.R. (1988). Evidence that luminal ER proteins are sorted from secreted proteins in a post-ER compartment. EMBO J. **7:** 913–918.

Pelham, H.R., Hardwick, K.G., and Lewis, M.J. (1988). Sorting of soluble ER proteins in yeast. EMBO J. **7:** 1757–1762.

Phillipson, B.A., Pimpl, P., daSilva, L.L., Crofts, A.J., Taylor, J.P., Movafeghi, A., Robinson, D.G., and Denecke, J. (2001). Secretory bulk flow of soluble proteins is efficient and COPII dependent. Plant Cell **13:** 2005–2020.

Pimpl, P., Hanton, S.L., Taylor, J.P., Pinto-daSilva, L.L., and Denecke, J. (2003). The GTPase ARF1p controls the sequence-specific vacuolar sorting route to the lytic vacuole. Plant Cell **15:** 1242–1256.

Pimpl, P., Taylor, J.P., Snowden, C., Hillmer, S., Robinson, D.G., and Denecke, J. (2006). Golgi-mediated vacuolar sorting of the endoplasmic reticulum chaperone BiP may play an active role in quality control within the secretory pathway. Plant Cell **18:** 198–211.

Rapoport, I., Chen, Y.C., Cupers, P., Shoelson, S.E., and Kirchhausen, T. (1998). Dileucine-based sorting signals bind to the beta chain of AP-1 at a site distinct and regulated differently from the tyrosine-based motif-binding site. EMBO J. **17:** 2148–2155.

Saint-Jean, B., Seveno-Carpentier, E., Alcon, C., Neuhaus, J.M., and Paris, N. (2010). The cytosolic tail dipeptide Ile-Met of the pea receptor BP80 is required for recycling from the prevacuole and for endocytosis. Plant Cell **22:** 2825–2837.

Sanderfoot, A.A., Ahmed, S.U., Marty-Mazars, D., Rapoport, I., Kirchhausen, T., Marty, F., and Raikhel, N.V. (1998). A putative vacuolar cargo receptor partially colocalizes with AtPEP12p on a prevacuolar compartment in Arabidopsis roots. Proc. Natl. Acad. Sci. USA **95:** 9920–9925.

Sauer, M., Delgadillo, M.O., Zouhar, J., Reynolds, G.D., Pennington, J.G., Jiang, L., Liljegren, S.J., Stierhof, Y.D., de Jaeger, G., Otegui,

M.S., Bednarek, S.Y., and Rojo, E. (2013). MTV1 and MTV4 encode plant-specific ENTH and ARF GAP proteins that mediate clathrin-dependent trafficking of vacuolar cargo from the trans-Golgi network. Plant Cell **25:** 2217–2235.

Scheuring, D., Viotti, C., Krüger, F., Künzl, F., Sturm, S., Bubeck, J., Hillmer, S., Frigerio, L., Robinson, D.G., Pimpl, P., and Schumacher, K. (2011). Multivesicular bodies mature from the trans-Golgi network/early endosome in *Arabidopsis*. Plant Cell **23:** 3463–3481.

Seaman, M.N., Marcusson, E.G., Cereghino, J.L., and Emr, S.D. (1997). Endosome to Golgi retrieval of the vacuolar protein sorting receptor, Vps10p, requires the function of the VPS29, VPS30, and VPS35 gene products. J. Cell Biol. **137:** 79–92.

Sevier, C.S., Weisz, O.A., Davis, M., and Machamer, C.E. (2000). Efficient export of the vesicular stomatitis virus G protein from the endoplasmic reticulum requires a signal in the cytoplasmic tail that includes both tyrosine-based and di-acidic motifs. Mol. Biol. Cell **11:** 13–22.

Shimada, T., Watanabe, E., Tamura, K., Hayashi, Y., Nishimura, M., and Hara-Nishimura, I. (2002). A vacuolar sorting receptor PV72 on the membrane of vesicles that accumulate precursors of seed storage proteins (PAC vesicles). Plant Cell Physiol. **43:** 1086–1095.

Sparkes, I.A., Runions, J., Kearns, A., and Hawes, C. (2006). Rapid, transient expression of fluorescent fusion proteins in tobacco plants and generation of stably transformed plants. Nat. Protoc. **1:** 2019–2025.

Stintzi, A., Heitz, T., Prasad, V., Wiedemann-Merdinoglu, S., Kauffmann, S., Geoffroy, P., Legrand, M., and Fritig, B. (1993). Plant 'pathogenesis-related' proteins and their role in defense against pathogens. Biochimie **75:** 687–706.

Takeuchi, M., Ueda, T., Sato, K., Abe, H., Nagata, T., and Nakano, A. (2000). A dominant negative mutant of sar1 GTPase inhibits protein transport from the endoplasmic reticulum to the Golgi apparatus in tobacco and Arabidopsis cultured cells. Plant J. **23:** 517–525.

Tanchak, M.A., Rennie, P.J., and Fowke, L.C. (1988). Ultrastructure of the partially coated reticulum and dictyosomes during endocytosis by soybean protoplasts. Planta **175:** 433–441.

Teeri, T.H., Lehväslaiho, H., Franck, M., Uotila, J., Heino, P., Palva, E.T., Van Montagu, M., and Herrera-Estrella, L. (1989). Gene fusions to lacZ reveal new expression patterns of chimeric genes in transgenic plants. EMBO J. **8:** 343–350.

Toyooka, K., Okamoto, T., and Minamikawa, T. (2000). Mass transport of proform of a KDEL-tailed cysteine proteinase (SH-EP) to protein storage vacuoles by endoplasmic reticulum-derived vesicle is involved in protein mobilization in germinating seeds. J. Cell Biol. **148:** 453–464.

Vitale, A., and Hinz, G. (2005). Sorting of proteins to storage vacuoles: How many mechanisms? Trends Plant Sci. **10:** 316–323.

Wang, H., Tse, Y.C., Law, A.H., Sun, S.S., Sun, Y.B., Xu, Z.F., Hillmer, S., Robinson, D.G., and Jiang, L. (2010). Vacuolar sorting receptors (VSRs) and secretory carrier membrane proteins (SCAMPs) are essential for pollen tube growth. Plant J. **61:** 826–838.

Wolfenstetter, S., Wirsching, P., Dotzauer, D., Schneider, S., and Sauer, N. (2012). Routes to the tonoplast: The sorting of tonoplast transporters in *Arabidopsis* mesophyll protoplasts. Plant Cell **24:** 215–232.

Xiang, L., and Van den Ende, W. (2013). Trafficking of plant vacuolar invertases: from a membrane-anchored to a soluble status. Understanding sorting information in their complex N-terminal motifs. Plant Cell Physiol. **54:** 1263–1277.